Radiocarbon analysis reveals underestimation of soil organic carbon persistence in new-generation soil models

Alexander Sohrab Brunmayr[1], Frank Hagedorn[2], Margaux Moreno Duborgel[2], Luisa Isabell Minich[2], and Heather Graven[1]

[1]Imperial College London
[2]Swiss Federal Institute for Forest, Snow and Landscape Research

December 10, 2023

Abstract

Reflecting recent advances in our understanding of soil organic carbon (SOC) turnover and persistence, a new generation of models increasingly makes the distinction between the more labile soil particulate organic matter (POM) and the more persistent mineral-associated organic matter (MAOM). Unlike the typically poorly defined conceptual pools of traditional SOC models, the POM and MAOM pools can be directly measured for their carbon content and isotopic composition, allowing for pool-specific data assimilation. However, the new-generation models' predictions of POM and MAOM dynamics have not yet been validated with pool-specific carbon and 14C observations. In this study, we evaluate 5 influential and actively developed new-generation models (CORPSE, Millennial, MEND, MIMICS, SOMic) with pool-specific and bulk soil 14C measurements of 77 mineral topsoil profiles in the International Soil Radiocarbon Database (ISRaD). We find that all 5 models consistently overestimate the 14C content (Δ14C) of POM by 67of the 5 models also strongly overestimate the Δ14C of MAOM by 74average, indicating that the models generally overestimate the turnover rates of SOC and do not adequately represent the long-term stabilization of carbon in soils. These results call for more widespread usage of pool-specific carbon and 14C measurements for parameter calibration, and may even suggest that some new-generation models might need to restructure their simulated pools (e.g. by adding inert pools to POM and MAOM) in order to accurately reproduce SOC dynamics.

Radiocarbon analysis reveals underestimation of soil organic carbon persistence in new-generation soil models

Alexander S. Brunmayr[1], Frank Hagedorn[2], Margaux Moreno Duborgel[2,3], Luisa I. Minich[2,3], Heather D. Graven[1]

[1]Imperial College London, Department of Physics
[2]Eidgenössische Forschungsanstalt WSL
[3]ETH Zurich, Department of Earth Sciences

Key Points:

- New-generation soil models generally overestimate ^{14}C content in topsoil.
- This may be because new-generation models have too fast turnover rates and do not include highly persistent compounds such as pyrogenic carbon.
- Discovery of more representative measurable pools is likely to improve new-generation model designs and performances with ^{14}C.

Corresponding author: Alexander S. Brunmayr, `asb219@ic.ac.uk`

Abstract

Reflecting recent advances in our understanding of soil organic carbon (SOC) turnover and persistence, a new generation of models increasingly makes the distinction between the more labile soil particulate organic matter (POM) and the more persistent mineral-associated organic matter (MAOM). Unlike the typically poorly defined conceptual pools of traditional SOC models, the POM and MAOM pools can be directly measured for their carbon content and isotopic composition, allowing for pool-specific data assimilation. However, the new-generation models' predictions of POM and MAOM dynamics have not yet been validated with pool-specific carbon and ^{14}C observations. In this study, we evaluate 5 influential and actively developed new-generation models (CORPSE, Millennial, MEND, MIMICS, SOMic) with pool-specific and bulk soil ^{14}C measurements of 77 mineral topsoil profiles in the International Soil Radiocarbon Database (ISRaD). We find that all 5 models consistently overestimate the ^{14}C content ($\Delta^{14}C$) of POM by 67‰ on average, and 3 out of the 5 models also strongly overestimate the $\Delta^{14}C$ of MAOM by 74‰ on average, indicating that the models generally overestimate the turnover rates of SOC and do not adequately represent the long-term stabilization of carbon in soils. These results call for more widespread usage of pool-specific carbon and ^{14}C measurements for parameter calibration, and may even suggest that some new-generation models might need to restructure their simulated pools (e.g. by adding inert pools to POM and MAOM) in order to accurately reproduce SOC dynamics.

1 Introduction

The terrestrial carbon reservoir sequesters an estimated 29% of anthropogenic CO_2 emissions each year (Friedlingstein et al., 2022), significantly reducing the accumulation rate of CO_2 in the atmosphere and thus slowing down climate change. However, the future role of the terrestrial carbon reservoir as a net CO_2 sink is uncertain, as Earth System Models (ESMs) produce a wide range of projections for the net land-atmosphere carbon flux over the course of the 21st century, partly due to high uncertainties in the carbon-climate feedback (Friedlingstein et al., 2014; Arora et al., 2020). Moreover, a study by He et al. (2016) using the radiocarbon (^{14}C) isotope suggests that some of the most widely used CMIP5 (Coupled Model Intercomparison Project Phase 5) ESMs may be systematically overestimating the future land carbon sink, further casting doubt on the reliability of future land sink predictions. All five ESMs tested in their study strongly underestimated the ^{14}C age of soil organic carbon, which indicates an overestimation of the simulated carbon cycling rates, particularly in the most stable soil carbon pools. After He et al. (2016) adjusted the soil carbon cycling rates to fit the observed ^{14}C data, the ESMs ended up predicting $40\pm27\,\%$ lower carbon sequestration by the terrestrial sink in the 21st century than with their default parameters. This result puts into question the ability of current ESMs to accurately model soil carbon dynamics, and highlights the importance of validating model predictions with ^{14}C data.

Almost all ESMs rely on soil organic carbon (SOC) modules that are ultimately based either on the Century model (Parton et al., 1987) (e.g., CESM2, Danabasoglu et al., 2020) or the RothC model (Coleman & Jenkinson, 1996) (e.g., JULES, Clark et al., 2011). Even though Century and RothC have been used for many decades to predict SOC dynamics in various landscapes with moderate success (Leifeld et al., 2008; Leifeld, 2008; Leifeld et al., 2009; Abramoff et al., 2022; H. Zhang et al., 2020), both modeling frameworks were developed in the 1980s, and thus reflect the comparatively limited understanding of soil carbon cycling of that time. Indeed, the model design of RothC is inspired by the now obsolete humification theory (Lehmann & Kleber, 2015; Schmidt et al., 2011), and neither RothC nor Century explicitly simulate specific processes of SOC cycling, such as physico-chemical protection of SOC or adsorption and desorption of dissolved organic carbon, because their mechanisms were previously not understood well enough.

According to our current understanding, the most important control on SOC stability is not so much the molecular composition or "quality" of organic matter, but rather its protection from microbial and abiotic decomposition through occlusion in aggregates and mineral association (Kleber et al., 2011; Dungait et al., 2012; Lehmann & Kleber, 2015; Lavallee et al., 2020). When SOC gets enclosed into aggregates or stabilized onto soil mineral surfaces through the action of pedogenic oxides, in particular iron, aluminum and calcium associated with clay particles (Rasmussen, Heckman, et al., 2018; Rowley et al., 2018; Vogel et al., 2014), it becomes less accessible to decomposers and thus significantly increases its residence time in soils (Basile-Doelsch et al., 2020; Schrumpf et al., 2013; Doetterl et al., 2015). A new generation of SOC models is now being developed to incorporate the theory of SOC protection through occlusion and interactions with soil minerals into our carbon cycle predictions. A common feature of new-generation soil models is their distinction between particulate organic matter (POM) and mineral-associated organic matter (MAOM). The POM pool largely consists of partially decomposed litter fragments smaller than 2 mm (Lavallee et al., 2020; Basile-Doelsch et al., 2020), which are usually covered with a thin mineral coating (Wagai et al., 2009). On the other hand, the MAOM pool contains organic matter chemically adsorbed onto reactive mineral surfaces, as well as strongly bound micro-aggregates formed around sand, silt, or clay particles (Basile-Doelsch et al., 2020; Lavallee et al., 2020). Unlike the carbon pools of RothC and Century, the POM and MAOM pools of the new-generation models can be operationally defined with experimental protocols by which they can be separated from soil samples and then analyzed individually for their elemental and isotopic composition (von Lützow et al., 2007). This allows for a closer look into the processes governing soil carbon stabilization and for potentially much larger datasets for model calibration and validation. However, the use of pool-specific measurements to validate models is still limited, even for new-generation models (Y. Zhang et al., 2021, Table S1).

The theory that protection and accessibility are the most important controls on SOC stability is strongly supported by ^{14}C studies (Gaudinski et al., 2000; Schrumpf et al., 2013, 2021), which could indicate that new-generation SOC models might perform better with ^{14}C than the traditional SOC models integrated into ESMs. ^{14}C is an effective carbon cycle tracer because it is chemically indistinguishable from the other carbon isotopes and therefore participates in the same carbon exchange mechanisms as the more abundant ^{12}C and ^{13}C isotopes. Over the past century, the atmospheric ^{14}C levels have undergone dramatic changes, most notably as a result of thermonuclear weapons tests in the 1950s and '60s, which have almost doubled the amount of atmospheric $^{14}CO_2$ in the Northern Hemisphere (see Figure 2). As this bomb-derived $^{14}CO_2$ spreads into the terrestrial carbon reservoirs through photosynthesis and into oceans through air-sea gas exchanges (Graven et al., 2020), the level of enrichment in bomb-derived ^{14}C across different terrestrial and oceanic carbon reservoirs helps to evaluate the speed and magnitude of carbon exchanges with the atmosphere on annual and decadal scales. Meanwhile for slower-cycling reservoirs such as deep soils or permafrost, the level of ^{14}C depletion due to radioactive decay (half-life of 5700±30 years (Roberts & Southon, 2007)) helps to estimate the time scales of carbon stabilization in those reservoirs on the order of centuries and millennia. ^{14}C is therefore a powerful tool to study the exchanges and storage of carbon from decadal to millennial time scales. However, new-generation models do not generally implement ^{14}C simulations, and only a handful have systematically assimilated observed ^{14}C data (e.g., Tipping & Rowe, 2019; Braakhekke et al., 2014; Ahrens et al., 2020).

In this study, we use ^{14}C measurements of the organic carbon in the mineral topsoil to evaluate the performance of five new-generation SOC models: CORPSE (Sulman et al., 2014), MEND-new (G. Wang et al., 2022), Millennial v2 (Abramoff et al., 2022), MIMICS-CN v1.0 (Kyker-Snowman et al., 2020), and SOMic 1.0 (Woolf & Lehmann, 2019). These models were chosen because they are open source, actively developed, and influential in the soil modeling community. Leveraging the measurability of their pools, we compare these models' predictions to ^{14}C measurements of POM and MAOM, in addition to the total soil ^{14}C. This provides a detailed picture of the modeled SOC dynamics and enables us to carry out an in-depth analysis of the models' performances.

2 Methods

Throughout this paper, we report the ^{14}C content of a given carbon sample as Δ^{14}C, which is the deviation of the sample's $^{14}C/^{12}C$ ratio from the "modern" standard, corresponding to the pre-industrial atmospheric $^{14}CO_2/^{12}CO_2$ ratio (Trumbore et al., 2016).

2.1 Pool-specific carbon and radiocarbon measurements

We compare model predictions to three types of measured data for the topsoil: (1) the total SOC stocks in the topsoil, (2) the relative mass contributions of POM and MAOM to the total SOC stocks, and (3) the Δ^{14}C of POM, MAOM, and bulk SOC.

For this study, we will use the International Soil Radiocarbon Database (ISRaD) (Lawrence et al., 2020) for carbon and ^{14}C measurements of POM and MAOM obtained from soil samples using a combination of density fractionation and ultra-sonication. Density fractionation with ultra-sonication is currently one of the most effective and commonly employed methods for separating POM and MAOM (Golchin et al., 1994; Griepentrog et al., 2015, 2014; Cerli et al., 2012; von Lützow et al., 2007; Poeplau et al., 2018). This method separates the soil into three "density fractions" – the free light fraction, occluded light fraction, and heavy fraction – in a three step process: (1) obtain the free light fraction from the soil sample by density fractionation; (2) in the remaining sample, destroy loosely-bound aggregates with ultra-sonication, thus releasing the occluded fraction; (3) isolate the occluded light fraction from the relatively denser heavy fraction by density fractionation. The resulting free and occluded light fractions correspond approximately to the POM pool, while the heavy fraction is a good proxy for the MAOM pool (Mikutta et al., 2019; Lavallee et al., 2020). We will from now on refer to the soil density fractions (light and heavy) by the names of the corresponding pools (POM and MAOM, respectively).

ISRaD provides carbon and ^{14}C data for the bulk soil, and the free light, occluded light, and heavy fractions. We derive the relative carbon contributions and Δ^{14}C of POM with a weighted average of the free and occluded light fractions, and we directly associate MAOM with the heavy fraction in ISRaD. When the Δ^{14}C of the bulk soil is not measured or reported in ISRaD, we calculate it with a weighted average of POM Δ^{14}C and MAOM Δ^{14}C. Since most of the available ^{14}C data is for the topsoil, we will evaluate models only for the top 5 cm or top 10 cm of the mineral soil. The current version of ISRaD (v 2.5.5.2023-09-20) contains complete ^{14}C datasets of the POM and MAOM density fractions in the topsoil of 77 soil profiles spread across 39 sampling sites, covering forests, shrubland, cultivated landscapes, and rangeland and grassland. Almost all of the sampling sites are in North America and Europe, and the remaining sites are located in Hawaii and Puerto Rico (see map in Figure 1). The dataset does not contain any permafrost, thermokarst, peatland, or wetland soils, and 75 of the 77 samples are from 1997-2015, with only one sample from 1949 and one sample from 1978. As shown in Figure 2, most datapoints bear a positive Δ^{14}C value, demonstrating an enrichment in bomb-derived ^{14}C in the topsoil.

2.2 Selection of new-generation models

We reviewed the literature to find new-generation models whose pools are fully compatible with the observed POM and MAOM density fractions, and that have already been tested with a range of soil types and environments. Table 1 gives an overview of the features and capabilities of such new-generation models, almost all of which have been de-

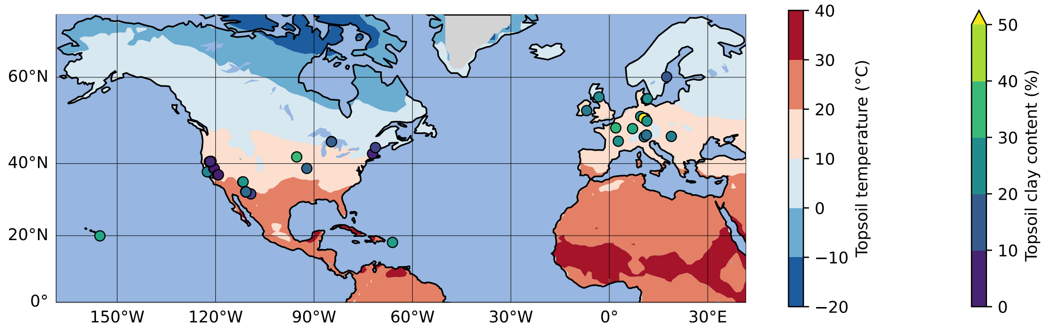

Figure 1. Map of selected topsoil sampling sites from ISRaD (Lawrence et al., 2020). 37 of the 39 sites are located in North America and Europe, and the two remaining sites are in Hawaii and Puerto Rico. All sites have a complete ^{14}C dataset for bulk soil and all density fractions for the top 5 or 10 cm of the mineral soil. The map also shows two of the most important environmental controls on soil carbon persistence: soil temperature (at 4 cm depth, averaged over 1970-2010 period, 1 degree horizontal resolution) from the CESM2 Large Ensemble product (Rodgers et al., 2021) on the map background, and clay content in the topsoil from ISRaD or SoilGrids (Poggio et al., 2021) for each sampling site.

veloped starting in the 2010s. Many new-generation SOC models also explicitly represent the microbial biomass as a separate carbon pool, since microbes are the main drivers of SOC turnover (Crowther et al., 2019; Basile-Doelsch et al., 2020; Schimel, 2023). The newest version of the MEND model simulates a variety of microbial exo-enzyme pools in addition to its microbial biomass pools (G. Wang et al., 2022). About half of the models listed in Table 1 have already been implemented with ^{14}C. However, none of them have systematically assimilated fraction-specific ^{14}C data, instead relying on ^{14}C data of bulk SOC or $^{14}CO_2$ data from soil respiration.

For this ^{14}C study, we chose to evaluate the following models, as their code is open-source and they have produced successful SOC predictions for a variety of ecosystems:

- Millennial v2 (with Michaelis-Menten kinetics), Abramoff et al. (2022),
- SOMic 1.0, Woolf and Lehmann (2019),
- MEND-new (with default equations), G. Wang et al. (2022),
- CORPSE (version from GitHub repository bsulman/CORPSE-fire-response), first described in Sulman et al. (2014),
- MIMICS-CN v1.0, Kyker-Snowman et al. (2020).

Figure 3 shows the general structure of the above models. All the selected models have pools which we can associate to the POM and MAOM fractions (see section S2 in the Supporting Information for details on how we associate the pools to each fraction), and they all have at least one microbial biomass pool. We generally chose to evaluate the most recent version of each model. However, we found an error in the ^{14}C implementation of the most recent version of MIMICS (Y. Wang et al., 2021) (see section S4.2 in the Supporting Information), so we chose to use the coupled carbon-nitrogen version MIMICS-CN published one year prior in Kyker-Snowman et al. (2020). See section S1 and Figures S1-S5 in the Supporting Information for more details on the exact versions and implementations of each model.

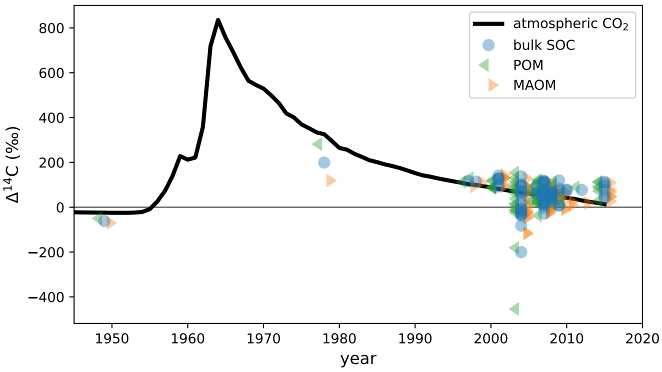

Figure 2. Measured $\Delta^{14}C$ data of the POM and MAOM density fractions and total soil organic carbon (SOC) at the selected topsoil profiles from ISRaD (Lawrence et al., 2020), overlaid on the atmospheric $\Delta^{14}CO_2$ curve of the Northern Hemisphere (Graven et al., 2017). All POM and MAOM fractions shown here were produced using the method of density fractionation with ultra-sonication. These ISRaD data were originally published in Baisden et al. (2002); Berhe et al. (2012); Harden et al. (2002); Heckman (2010); Heckman et al. (2018); Lybrand et al. (2017); Marín-Spiotta et al. (2008); McFarlane et al. (2013); Meyer et al. (2012); Rasmussen, Throckmorton, et al. (2018); Schrumpf et al. (2013).

Note that the MIND model (Fan et al., 2021) would have been a great candidate for evaluation, too, but only a subset of the modeled pools was run globally, so some of its parameters (e.g. $V_{\max,P}$ and $K_{M,P}$) do not have fitted values outside of 4 experimental test cases.

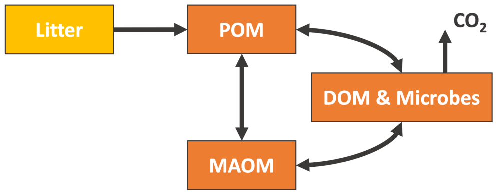

Figure 3. General structure of the new-generation models which we chose for this study. The MIMICS and CORPSE models additionally feature a CO_2 flux leaving MAOM and POM, which depends on the carbon use efficiency of the microbes. The SOMic and CORPSE models do not allow any flux from the DOM, Microbe, or MAOM pools back into the POM pool. More detailed diagrams for the MEND, Millennial, SOMic, CORPSE, and MIMICS models can be found in the Supporting Information (Figures S1-S5). Abbreviations: POM = particulate organic matter ; MAOM = mineral-associated organic matter ; DOM = dissolved organic matter.

2.3 Model input data

For each measurement site, the models are run with local environmental forcing data from 1850 to 2014. The initial conditions in 1850 are found by spinning up the models, looping over a "pre-industrial" year, where the forcing data is averaged over the 1850-1879 period, until the system reaches equilibrium, i.e. does not experience any signifi-

Table 1. Summary of features and capabilities of new-generation models. All of the listed models are compatible with the distinction between POM and MAOM and have been used to produce predictions for a variety of soil profiles. The models selected for evaluation with ^{14}C in this study are indicated with an asterisk ($*$). The first two columns are the year of the first publication and, if applicable, the year of the latest published revision of each model at the time of writing. The "Open-source," "Implements ^{14}C," and "Explicitly models" columns are checkmarked if at least one version of the model has open-source code, implements ^{14}C simulations, or explicitly models a specified pool or feature, respectively. In the "Vertical mixing" subcolumn, models with a downward arrow (↓) simulate any kind of downward transport or leaching for at least one of their pools, often in dissolved form, and sometimes using an advection equation. Models featuring an up-down arrow (↕) additionally implement vertical mixing for at least one of their pools with a diffusion equation.

					Explicitly models				
Model name	First publication	Latest revision	Open-source	Implements ^{14}C	DOM	Microbes	Enzymes	Vertical mixing	Notes
$*$ Millennial [1]	2018	2022	✓		✓	✓		↓	
$*$ SOMic [2]	2019		✓	✓	✓	✓		↓	
$*$ MEND [3]	2013	2022	✓	✓	✓	✓	✓		^{14}C only in 2015
$*$ CORPSE [4]	2014	2020	✓			✓			
$*$ MIMICS [5]	2014	2021	✓	✓		✓		↓↕	^{14}C and ↓↕ only in 2021
MIND [6]	2021		✓			✓			
AggModel [7]	2013		✓						incubation model
JSM [8]	2020		(✓)	✓	✓	✓		↓↕	source code accessible upon request
COMISSION [9]	2015	2020		✓	✓	✓		↓↕	^{14}C introduced in v2.0
Tipping & Rowe [10]	2019			✓	✓			↓	
MEMS [11]	2019	2021			✓	✓		↓↕	↕ introduced in v2.0
SOMPROF [12]	2011	2014		✓				↓↕	^{14}C introduced in 2014
CAST [13]	2013							↓	
Struc-C [14]	2009								
PROCAAS [15]	2020								incubation model

[1]Abramoff et al. (2018, 2022) ; [2]Woolf and Lehmann (2019) ; [3]G. Wang et al. (2013, 2015, 2022) ; [4]Sulman et al. (2014, 2017); Salazar et al. (2018); Hicks Pries et al. (2018); Moore et al. (2020) ; [5]Wieder et al. (2014, 2015); H. Zhang et al. (2020); Kyker-Snowman et al. (2020); Y. Wang et al. (2021) ; [6]Fan et al. (2021) ; [7]Segoli et al. (2013) ; [8]Yu et al. (2020) ; [9]Ahrens et al. (2015, 2020) ; [10]Tipping and Rowe (2019) ; [11]Robertson et al. (2019); Y. Zhang et al. (2021) ; [12]Braakhekke et al. (2011, 2013, 2014) ; [13]Stamati et al. (2013) ; [14]Malamoud et al. (2009) ; [15]Liu et al. (2020)

cant inter-annual variability. More details on the spinup methods for each model are given in section S1 in the Supporting Information.

The selected models require a number of constant and time-dependent forcing data to be run at each study site. We assume that soil properties such as sand, clay and silt content, soil density, and land use are time-invariant since pre-industrial times. Where these site-specific soil properties are not reported in ISRaD, they are taken from the SoilGrids database (Poggio et al., 2021). The MIMICS model also requires the lignin content of litter inputs, which we set to be a constant value depending only on the land use type. We assume that the lignin content is 25% for forest litter and 7% for shrubland litter (Rahman et al., 2013, Table 1). For grassland and cultivated landscapes, we assume a lignin content of 9% based on measurements of grasses at the seeding stage (Armstrong et al., 1950, Table 1). Weather-dependent and other dynamic environmental properties, such as soil temperature and ^{14}C influx, are taken from global model predictions with monthly time resolution. We use the monthly averaged CESM2 Large Ensemble (CESM2-LE) product (Rodgers et al., 2021) for vertically resolved soil temperature and moisture, above- and below-ground net primary production (NPP), total gross primary productivity (GPP), and the carbon-to-nitrogen ratio and $\Delta^{14}C$ of total litter carbon from 1850 to 2014 with 1 degree spatial resolution. Since the below-ground NPP from the CESM2-LE output is not vertically resolved, we derive the topsoil portion of the below-ground NPP using the exponential function model from Xiao et al. (2023). For nitrogen deposition rates, we use monthly data simulated by the NCAR Chemistry-Climate Model Initiative (CCMI) on a 0.5 degree grid from 1860 to 2016 (Tian et al., 2018). We extend this data back to 1850 by setting the monthly nitrogen deposition rates for the 1850-1860 period to be equal to the average monthly rates over the 1860-1870 period.

Since none of the selected models represent lateral carbon transport or upward vertical mixing of soil carbon, the simulated topsoil systems receive all of their carbon exclusively from vegetation inputs. We can therefore estimate the carbon influx into the soil with the NPP, and the $\Delta^{14}C$ of the influx with the $\Delta^{14}C$ of litter from the CESM2-LE product. In the case of the MEND model, we use GPP instead of NPP as a model input, as prescribed by MEND's developers.

3 Results

We produced carbon and ^{14}C predictions with the MEND, Millennial, SOMic, CORPSE and MIMICS models for the 77 selected soil profiles, and compared them to the observed carbon and ^{14}C data from ISRaD. Our main performance metrics are the root mean squared error (RMSE) and mean bias of the predictions with respect to the 6 observational datasets described in Section 2.1. Table 2 gives a summary of the model performances, and Figures S8-S12 in the Supporting Information show plots of predictions against observations for each variable and each model. Note that the MEND model failed to run on 12 of the 77 selected soil profiles due to some numerical instability, and was unable to produce ^{14}C data for 3 other profiles. Note also that the SOC stocks for 17 of the 77 selected profiles are not available in ISRaD.

3.1 Carbon stocks and partitioning between pools

The SOMic, Millennial, and CORPSE models tend to overestimate the topsoil SOC stocks of the selected soil profiles, while MEND and MIMICS underestimate the SOC stocks, as shown in Figure 4a. In their predictions of SOC partitioning into POM and MAOM, the new-generation models generally fail to cover the full range of variability in the observations, with the exception of the MIMICS model (see Figure 4b-c). The CORPSE and MIMICS models perform the best, and both have a RMSE of around 20 percentage points, and a bias of around 10 points or less in magnitude. Meanwhile, the remaining models have an average RMSE of 35 points and an average absolute bias of around 25 points in their predictions of POM and MAOM contributions to total SOC stocks (see Table 2).

Table 2. Root mean squared error (RMSE) and mean bias for each model and each dataset. In the case of the MEND model, the RMSE and bias were calculated based on results of $n = 62$ profiles for the $\Delta^{14}C$ rows, $n = 52$ for SOC stocks, and $n = 65$ for the rows of POM and MAOM contributions. For all other models, $n = 77$ for all rows, except SOC stocks, where $n = 60$.

		MEND	Millennial	SOMic	CORPSE	MIMICS	Average
Bulk SOC $\Delta^{14}C$ (‰)	RMSE	84	115	101	90	80	94
	Bias	+59	+69	+46	+35	0	+42
POM $\Delta^{14}C$ (‰)	RMSE	94	120	100	119	129	112
	Bias	+50	+63	+56	+86	+80	+67
MAOM $\Delta^{14}C$ (‰)	RMSE	103	117	102	83	74	96
	Bias	+83	+82	+57	-3	-39	+36
SOC stocks (kgC/m^2)	RMSE	4.1	3.8	3.2	6.2	2.3	3.9
	Bias	−1.3	+2.7	+1.9	+4.0	−1.6	+1.1
POM contribution (%)	RMSE	35	40	32	23	17	29
	Bias	+24	−33	−22	+11	−2	−4
MAOM contribution (%)	RMSE	35	41	30	21	21	30
	Bias	−24	+35	+20	−9	−9	+2

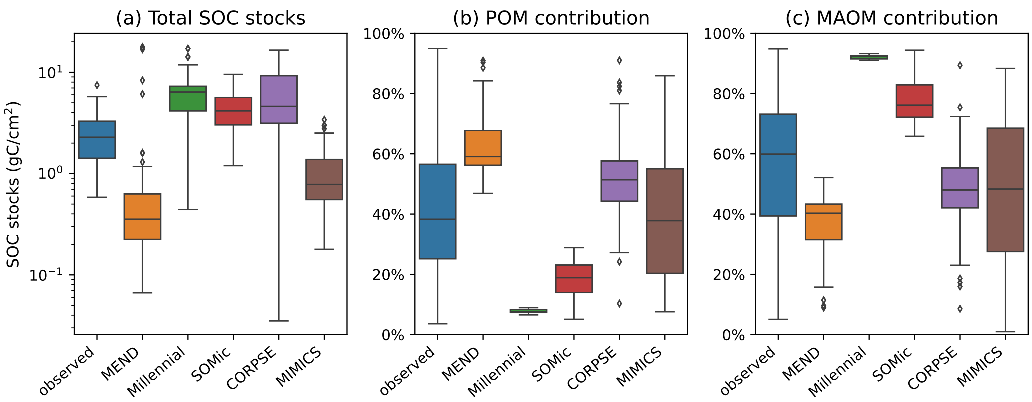

Figure 4. Observed and modeled total SOC stocks in the topsoil (top 5 or 10 cm of mineral soil) plotted on a log-transformed axis in subplot (a), and contributions of the POM and MAOM pools to the topsoil SOC stocks in subplots (b) and (c), respectively. Black diamonds are outliers. In (a), $n = 60$ for the boxplot of observed data, $n = 65$ for MEND, and $n = 77$ for all other models. In (b) and (c), $n = 77$ for all boxplots, except for MEND, where $n = 65$.

3.2 Performance with ^{14}C

With the notable exception of MIMICS, the new-generation models consistently overestimate the $\Delta^{14}C$ of bulk SOC, and their ^{14}C predictions do not capture the full variability of the observations (see Figure 5a). This is reminiscent of the ESMs' ^{14}C predictions (He et al., 2016), which also overestimate the $\Delta^{14}C$ of SOC and underestimate its variability. Therefore, our results could suggest that the new generation of soil models may be facing similar issues as the traditional SOC models incorporated into ESMs.

The pool-specific ^{14}C results, shown in Figure 5b-c, shed a more critical light on the performance of MIMICS with the $\Delta^{14}C$ of bulk SOC. MIMICS overestimates the $\Delta^{14}C$

of POM by 80‰ and underestimates the $\Delta^{14}C$ of MAOM by around 40‰ on average, and these biases happen to cancel out in such a way that MIMICS produces very good predictions for the $\Delta^{14}C$ of bulk SOC with a RMSE of just 80‰ and no bias, the best performance among the evaluated models (see Table 2). All five models overestimate the $\Delta^{14}C$ of POM, with an average positive bias of 67‰, and SOMic, Millennial, and MEND also overestimate MAOM $\Delta^{14}C$ by 74‰ on average. CORPSE is good at predicting the $\Delta^{14}C$ of MAOM with effectively no bias, but its POM $\Delta^{14}C$ predictions have the largest bias (+119‰) among all the models. On average, the evaluated models have a positive bias between 36‰ and 67‰, and a RMSE around 100‰ in their $\Delta^{14}C$ predictions for the POM, MAOM, and bulk SOC (see Table 2 for more details).

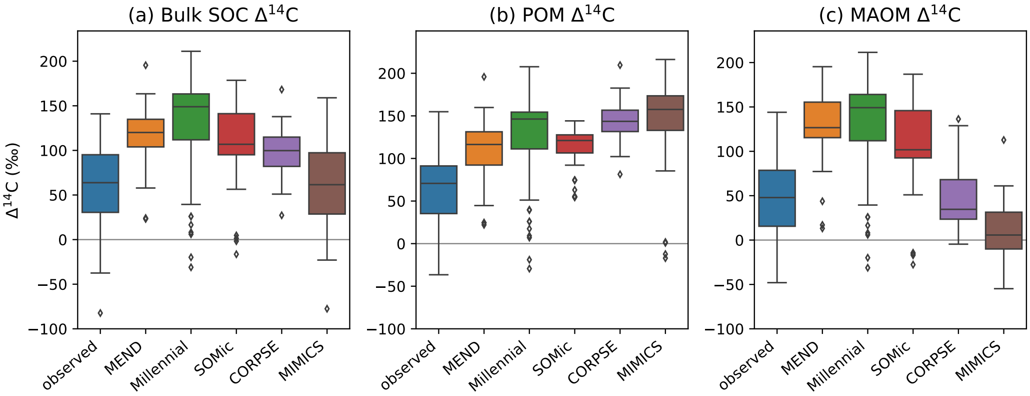

Figure 5. Observed and modeled $\Delta^{14}C$ of total SOC (a), POM (b), and MAOM (c) in the topsoil (top 5 or 10 cm of mineral soil). Black diamonds are outliers. Note that some extreme outliers are outside of plotting range. To have a uniform and consistent ^{14}C dataset, we excluded the 1949 and 1978 samples so that we end up with more compact data spanning only 18 years at the tail end of the bomb spike. Therefore, $n = 75$ for all boxplots, except for MEND's, where $n = 62$.

The models produce contrasting predictions for the evolution of soil ^{14}C over the second half of the 20th century. In the example of an alpine pasture (Figure 6), we can see that the CORPSE, SOMic and MIMICS models predict $\Delta^{14}C$ curves for POM which are distinct from MAOM, while the MEND and Millennial models produce similar $\Delta^{14}C$ dynamics for POM and MAOM. That is because the Millennial and MEND models have faster turnover rates than the other models, and their pools rapidly exchange carbon between themselves.

3.3 Role of environmental parameters

We further investigate how simulations depend on soil temperature and clay content, as these are considered some of the most important factors controlling SOC turnover and persistence (Basile-Doelsch et al., 2020; Leifeld et al., 2009).

Higher soil temperatures enhance microbial activity and generally increase the turnover rate of carbon in soils (German et al., 2012; Leifeld et al., 2009; Sierra et al., 2015). While the observed SOC stocks and POM and MAOM contributions are not correlated with temperature (Figure 7a-c), the observed $\Delta^{14}C$ of POM, MAOM, and bulk SOC significantly increase with higher temperature (Figure 7d-f), probably due to shorter carbon residence times in warmer soils. In contrast, the predicted $\Delta^{14}C$ of POM, MAOM, and bulk SOC are either uncorrelated or negatively correlated with soil temperature. All of

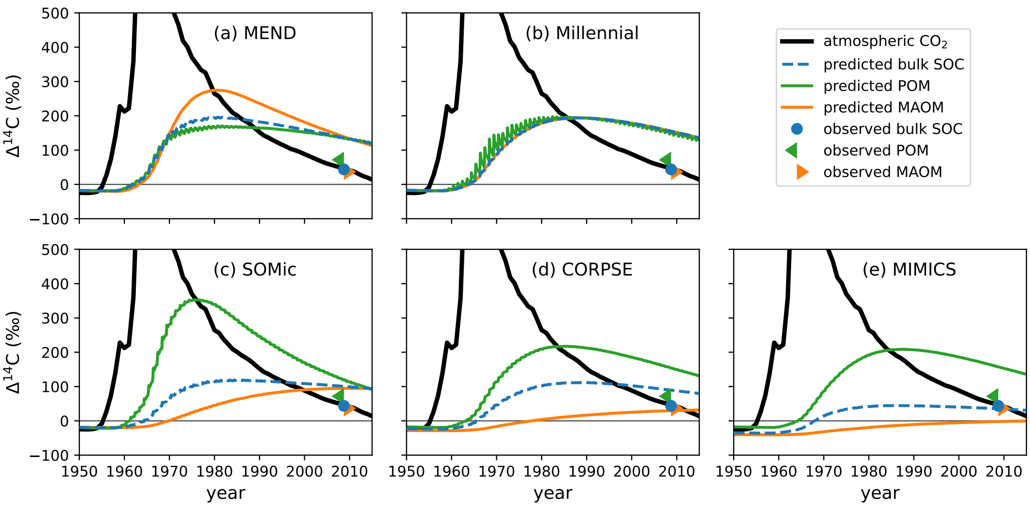

Figure 6. Observed and predicted Δ^{14}C of POM, MAOM, and bulk SOC in the top 10 cm of the mineral soil of a pasture in the Matsch valley, Italy. The observed ^{14}C data from 2008 are published in Meyer et al. (2012). The atmospheric $\Delta^{14}CO_2$ of the Northern Hemisphere (Graven et al., 2017) is shown for reference. With the SOMic, CORPSE and MIMICS models, the predicted Δ^{14}C of POM is distinct from the predicted Δ^{14}C of MAOM. On the other hand, the POM and MAOM pools in MEND and Millennial have very similar Δ^{14}C signals throughout the bomb-spike period.

the selected models modify carbon decomposition rates with a temperature-dependent scaling factor (Abramoff et al., 2022; Woolf & Lehmann, 2019; Kyker-Snowman et al., 2020; G. Wang et al., 2022; Sulman et al., 2014), but these results could indicate that they may need to increase or change the effect of temperature on carbon turnover rates.

In Figure 8c, the clay content of the sampled topsoils seems to be a decisive factor controlling the observed contribution of MAOM carbon to the total SOC stocks, with higher clay content correlating with higher MAOM contribution. This is also true for the MAOM contributions predicted by the MIMICS and CORPSE models, which produce the most accurate predictions of MAOM contribution (see Table 2). However, MIMICS appears to struggle with correctly simulating the effects of increased clay content on overall SOC dynamics, as evidenced by the inaccurate relationships of SOC stocks and Δ^{14}C with clay (see Figure 8a and Figure 8d-f). It appears that MIMICS correctly reproduces the evolution of MAOM contribution with clay content by increasing the residence time of carbon in MAOM, which in turn lowers the Δ^{14}C of MAOM and increases SOC stocks, contrary to the observations.

4 Discussion

The comparison of new-generation model predictions with ^{14}C observations reveals inaccuracies in the estimations of the time scales of carbon exchanges and stabilization in soils. Just like ESMs, most new-generation models overestimate the Δ^{14}C of bulk soil organic carbon (SOC) and they, too, may therefore be overestimating the effectiveness of soils as a net atmospheric CO_2 sink in the 21st century (He et al., 2016). The biases in the predictions of the repartition of SOC between particulate organic matter (POM) and mineral-associated organic matter (MAOM) may also affect the accuracy of future projections. POM and MAOM have been shown to have different sensitivities to envi-

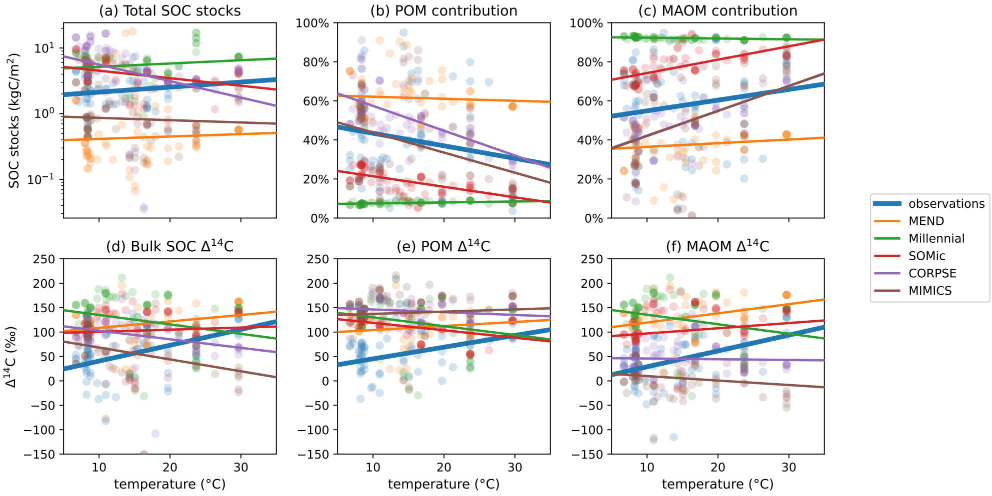

Figure 7. Relationship of observed and predicted carbon and Δ^{14}C data with respect to mean annual temperature of the topsoil (averaged over the 1970-2010 period). Circles are datapoints, and lines are best linear fits through the points. The observed Δ^{14}C of bulk SOC, POM, and MAOM have a strong positive relationship with temperature. Meanwhile, the predicted Δ^{14}C are more weakly and sometimes negatively correlated with temperature. The linear fit line of CORPSE in subplot (c) is completely covered by the linear fit line of MIMICS. Note that we once again excluded the 1949 and 1978 samples for these plots.

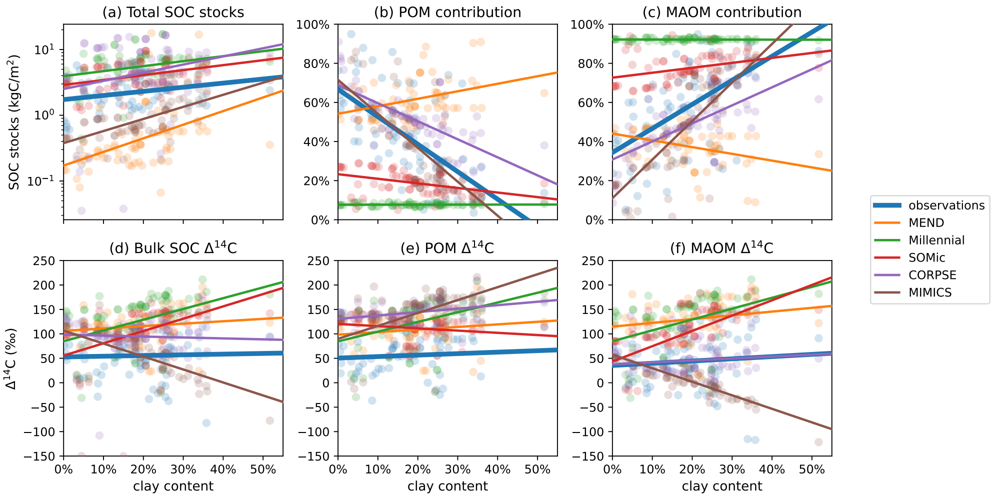

Figure 8. Relationship of observed and predicted carbon and Δ^{14}C data with respect to clay content in the topsoil. Circles are datapoints, and lines are best linear fits through the points. CORPSE and MIMICS successfully reproduce the positive relationship between topsoil clay content and the observed MAOM contribution to total SOC stocks in subplot (c). However, in subplot (f), MIMICS has a strong negative correlation of MAOM Δ^{14}C with clay content, unlike the observations, which do not show a correlation. The linear fit line of CORPSE in subplot (f) overlaps with that of the observations. Note that we once again excluded the 1949 and 1978 samples for these plots.

ronmental variables such as temperature and are thus expected to react differently to a changing climate (Hicks Pries et al., 2017; Kleber et al., 2011). Therefore, if models do not correctly partition SOC into POM and MAOM and misrepresent their ^{14}C, they will probably produce inaccurate predictions of SOC dynamics under climate change.

We identify three likely reasons why the new-generation models generally underperform with ^{14}C, and discuss how these problems could potentially be solved:

1. Insufficient datasets for the calibration of carbon turnover rates,
2. Lack of a "passive" pool with very slow turnover to account for inert SOC components,
3. Modeled pools do not capture the full range of SOC turnover rates.

The last point raises questions on the effectiveness of the new-generation models and the POM-MAOM distinction as a whole. This invites further research on the stability of the different constituents of SOC and a discussion on the most effective way to partition SOC into representative measurable pools.

4.1 Insufficient calibration datasets

Our ^{14}C results suggest that the new-generation models selected for this study overestimate some carbon turnover rates. The most extreme case is Millennial v2, which gives its micro-aggregate pool and mineral-adsorbed carbon pool turnover times of just a few months (see section S5 of supplement). On the other hand, ^{14}C-based studies find that the MAOM fraction, which includes micro-aggregates and mineral-adsorbed carbon, typically turns over on time scales of many decades or centuries (Gaudinski et al., 2000; Schrumpf & Kaiser, 2015; van der Voort et al., 2017; Baisden et al., 2002). The overestimation of turnover rates may be due to inadequate or insufficient data for the calibration of the models' turnover parameters. Even though new-generation models have measurable pools, they do not usually assimilate pool-specific carbon and ^{14}C data, probably because such data are currently very sparse. The only models in our evaluation to calibrate their parameters with pool-specific carbon data are CORPSE (with data from only 2 soil profiles, according to Y. Zhang et al., 2021, Table S1) and Millennial (as described in Abramoff et al., 2022), and none of them assimilated pool-specific ^{14}C data. Instead, new-generation models primarily rely on less informative bulk soil data, as well as some soil incubation results, for parameter optimization. However, as the dataset of fraction-specific carbon and ^{14}C measurements is growing larger, new-generation models should start to take full advantage of the measurability of their pools and assimilate those highly informative data.

4.2 Lack of passive pool

Another explanation for the consistent overestimation of soil Δ^{14}C by new-generation models is the inability of the models to account for the presence of practically inert compounds in the soil, which negatively offset the bulk Δ^{14}C. For example, some soils with a history of wildfires may contain a considerable fraction of pyrogenic carbon, which is composed of highly durable aromatic compounds and can remain in soils over thousands of years (Eckmeier et al., 2009; Hajdas et al., 2007; Leifeld, 2008). Due to its extreme longevity, pyrogenic carbon is depleted in ^{14}C as a result of radioactive decay, bringing down the overall Δ^{14}C of both POM (van der Voort et al., 2017) and MAOM (Soucémarianadin et al., 2019). In deeper soils, the Δ^{14}C of SOC can be even further depleted due to a larger proportion of petrogenic carbon, which is devoid of ^{14}C (van der Voort et al., 2019). Whereas the two major traditional SOC models explicitly account for such extremely old components with a "passive" pool (1000 year turnover time) in the Century model (Parton et al., 1987) and an "inert organic matter" pool (no turnover at all) in the RothC model (Coleman & Jenkinson, 1996), the new-generation models effectively force virtually inert components to fit into their actively cycling carbon pools. By creating a passive pool to account for inert compounds such as pyrogenic carbon, the new-generation models would be able to lower the overall $\Delta^{14}C$ of POM and MAOM, and more accurately reproduce the measured ^{14}C data.

4.3 Search for more representative measurable pools

Finally, the underperformance of the models with respect to ^{14}C may also be due to a choice of pools which are not truly representative of the full spectrum of turnover rates of the different SOC components. Whereas traditional models simply define the number and turnover rates of their SOC pools such that they can reproduce observed SOC dynamics while minimizing degrees of freedom, new-generation models also need to make sure their pools are at once easily measurable and representative of the various time scales of soil carbon persistence. If a measurable pool contains two or more components with very different turnover rates, the model may not be able to correctly reproduce the $\Delta^{14}C$ of that pool because it assumes a single, homogeneous turnover rate for the entire carbon pool. Although some models already split POM into various subpools with contrasting turnover times (e.g., soluble and insoluble litter pools in SOMic, or oxidizable and hydrolysable POM pools in MEND), they miss the most recalcitrant POM pool of pyrogenic carbon, which even in minute amounts can significantly alter the $\Delta^{14}C$ and apparent turnover of POM (Leifeld, 2008). Some new-generation models subdivide the MAOM pool into micro-aggregates and mineral-adsorbed carbon (e.g., Millennial), or into an active layer of adsorbed DOC and a more stable MAOM component (e.g., MEND). However, those MAOM subpools might still not be homogeneous enough in their turnover times for effective ^{14}C simulations. Recent ^{14}C studies determining the stability of MAOM under the action of peroxide oxidation show that it may be necessary to further split clay-sized MAOM into two measurable subpools which are decomposable or resistant to microbial exo-enzymes (Schrumpf et al., 2021; Jagadamma et al., 2010). Additionally, "continuous" SOC fractionation methods such as ramped pyrolysis oxidation (Stoner et al., 2023) could provide a much higher resolution of the SOC turnover rate spectrum. However, the resulting measurable pools are more difficult to interpret in terms of their role in the soil carbon cycle, and their incorporation into mechanistic SOC models is therefore less straightforward.

4.4 Limitations of this study

The accuracy of our model evaluation is affected by multiple factors. Though we took care to accurately match the modeled pools to the measured fractions (see section S2 in Supporting Information), the correspondences are imperfect and further complicated by non-standardized definitions and density cut-offs for the light and heavy fractions published on ISRaD. Nevertheless, this does not change the overall overestimation of soil $\Delta^{14}C$ by most models. The use of forcing data from possibly inaccurate CESM2-LE and CCMI outputs with low spatial resolution may also affect the accuracy of our model evaluation. Furthermore, the $\Delta^{14}C$ of the carbon inputs from the CESM2-LE product could be inaccurate, especially in soils with a thick organic layer, which pre-ages the carbon before it enters the mineral soil. However, the consistency and magnitude of the models' overestimation of the topsoil's $\Delta^{14}C$ with respect to observed data indicate that this overestimation is evidently a real pattern among the studied models. Finally, it is also important to note that our study only produces an incomplete picture of model performances on a global scale, since most of the measured datapoints represent North American and European forest ecosystems.

5 Summary

Despite their incorporation of the latest advances in soil sciences, new-generation soil organic carbon (SOC) models currently show similar discrepancies with ^{14}C data as the traditional SOC models. The new-generation models' consistent overestimation of the Δ^{14}C in both particulate organic matter (POM) and mineral-associated organic matter (MAOM) and their inaccurate partitioning of SOC between POM and MAOM suggest that these models underestimate the time scales of carbon storage in soils and might produce unreliable future predictions under climate change. To improve their predictions, new-generation models should take advantage of the measurability of their pools and calibrate their parameters with the rapidly growing dataset of pool-specific carbon and ^{14}C measurements in addition to incubation and bulk soil data. They may also have to reconsider their model design and simulate measurable pools which better capture the full spectrum of carbon turnover rates present in the soils. In particular, the consideration of highly persistent soil carbon such as pyrogenic carbon could significantly improve ^{14}C predictions. As more effective measurable pools are being discovered and the dataset of pool-specific ^{14}C data is expanding, new-generation soil models have the potential to eventually supersede the traditional SOC models employed by ESMs if they take full advantage of the measurability of their pools and assimilate the available data.

6 Open Research

The source code to download the input data, run the models, and reproduce all the results presented in this manuscript is available on our GitHub repository `https://github.com/asb219/evaluate-SOC-models`.

Our final implementations of Millennial, CORPSE, MIMICS, and the ^{14}C component of MEND are available as python modules in our repository. For the carbon and nitrogen components of MEND, the Fortran source code is in `https://github.com/asb219/MEND` (forked from `https://github.com/wanggangsheng/MEND`), which is added as a "git submodule" to our repository. We use the `install_github` function of the `devtools` package in R to compile the C++ code of the SOMic model released as "v1.1-asb219" in `https://github.com/asb219/somic1` (forked from `https://github.com/domwoolf/somic1`) and install it as an R package. We download data from SoilGrids with the `soilgrids` python package (`https://github.com/gantian127/soilgrids`).

Acknowledgments

This study was supported by the Swiss National Science Foundation through the Sinergia scheme (grant no. 193770).

References

Abramoff, R. Z., Guenet, B., Zhang, H., Georgiou, K., Xu, X., Viscarra Rossel, R. A., ... Ciais, P. (2022, January). Improved global-scale predictions of soil carbon stocks with Millennial Version 2. *Soil Biology and Biochemistry*, *164*, 108466. Retrieved 2022-01-19, from `https://linkinghub.elsevier.com/retrieve/pii/S0038071721003400` doi: 10.1016/j.soilbio.2021.108466

Abramoff, R. Z., Xu, X., Hartman, M., O'Brien, S., Feng, W., Davidson, E., ... Mayes, M. A. (2018, January). The Millennial model: in search of measurable pools and transformations for modeling soil carbon in the new century. *Biogeochemistry*, *137*(1-2), 51–71. Retrieved 2021-03-21, from `http://link.springer.com/10.1007/s10533-017-0409-7` doi: 10.1007/s10533-017-0409-7

Ahrens, B., Braakhekke, M. C., Guggenberger, G., Schrumpf, M., & Reichstein, M.

(2015, September). Contribution of sorption, DOC transport and microbial interactions to the 14C age of a soil organic carbon profile: Insights from a calibrated process model. *Soil Biology and Biochemistry*, *88*, 390–402. Retrieved 2022-05-29, from https://linkinghub.elsevier.com/retrieve/pii/S0038071715002138 doi: 10.1016/j.soilbio.2015.06.008

Ahrens, B., Guggenberger, G., Rethemeyer, J., John, S., Marschner, B., Heinze, S., ... Schrumpf, M. (2020, September). Combination of energy limitation and sorption capacity explains 14C depth gradients. *Soil Biology and Biochemistry*, *148*, 107912. Retrieved 2022-07-10, from https://linkinghub.elsevier.com/retrieve/pii/S0038071720302091 doi: 10.1016/j.soilbio.2020.107912

Armstrong, D. G., Cook, H., & Thomas, B. (1950, January). The lignin and cellulose contents of certain grassland species at different stages of growth. *The Journal of Agricultural Science*, *40*(1-2), 93–99. Retrieved 2023-11-25, from https://www.cambridge.org/core/product/identifier/S002185960004555X/type/journal_article doi: 10.1017/S002185960004555X

Arora, V. K., Katavouta, A., Williams, R. G., Jones, C. D., Brovkin, V., Friedlingstein, P., ... Ziehn, T. (2020, August). Carbon–concentration and carbon–climate feedbacks in CMIP6 models and their comparison to CMIP5 models. *Biogeosciences*, *17*(16), 4173–4222. Retrieved 2023-03-09, from https://bg.copernicus.org/articles/17/4173/2020/ doi: 10.5194/bg-17-4173-2020

Baisden, W. T., Amundson, R., Cook, A. C., & Brenner, D. L. (2002, December). Turnover and storage of C and N in five density fractions from California annual grassland surface soils: TURNOVER AND STORAGE OF C AND N. *Global Biogeochemical Cycles*, *16*(4), 64–1–64–16. Retrieved 2023-07-01, from http://doi.wiley.com/10.1029/2001GB001822 doi: 10.1029/2001GB001822

Basile-Doelsch, I., Balesdent, J., & Pellerin, S. (2020, October). Reviews and syntheses: The mechanisms underlying carbon storage in soil. *Biogeosciences*, *17*(21), 5223–5242. Retrieved 2023-08-28, from https://bg.copernicus.org/articles/17/5223/2020/ doi: 10.5194/bg-17-5223-2020

Berhe, A. A., Harden, J. W., Torn, M. S., Kleber, M., Burton, S. D., & Harte, J. (2012, June). Persistence of soil organic matter in eroding versus depositional landform positions: EROSION AND SOIL ORGANIC MATTER DYNAMICS. *Journal of Geophysical Research: Biogeosciences*, *117*(G2), n/a–n/a. Retrieved 2023-07-01, from http://doi.wiley.com/10.1029/2011JG001790 doi: 10.1029/2011JG001790

Braakhekke, M. C., Beer, C., Hoosbeek, M. R., Reichstein, M., Kruijt, B., Schrumpf, M., & Kabat, P. (2011, May). SOMPROF: A vertically explicit soil organic matter model. *Ecological Modelling*, *222*(10), 1712–1730. Retrieved 2021-04-21, from https://linkinghub.elsevier.com/retrieve/pii/S0304380011000962 doi: 10.1016/j.ecolmodel.2011.02.015

Braakhekke, M. C., Beer, C., Schrumpf, M., Ekici, A., Ahrens, B., Hoosbeek, M. R., ... Reichstein, M. (2014, March). The use of radiocarbon to constrain current and future soil organic matter turnover and transport in a temperate forest. *Journal of Geophysical Research: Biogeosciences*, *119*(3), 372–391. Retrieved 2021-04-21, from http://doi.wiley.com/10.1002/2013JG002420 doi: 10.1002/2013JG002420

Braakhekke, M. C., Wutzler, T., Beer, C., Kattge, J., Schrumpf, M., Ahrens, B., ... Reichstein, M. (2013, January). Modeling the vertical soil organic matter profile using Bayesian parameter estimation. *Biogeosciences*, *10*(1), 399–420. Retrieved 2021-04-21, from https://bg.copernicus.org/articles/10/399/2013/ doi: 10.5194/bg-10-399-2013

Cerli, C., Celi, L., Kalbitz, K., Guggenberger, G., & Kaiser, K. (2012, January). Separation of light and heavy organic matter fractions in soil — Testing for proper density cut-off and dispersion level. *Geoderma*, *170*, 403–416. Retrieved 2022-01-23, from https://linkinghub.elsevier.com/retrieve/pii/S0016706111002941 doi: 10.1016/j.geoderma.2011.10.009

Clark, D. B., Mercado, L. M., Sitch, S., Jones, C. D., Gedney, N., Best, M. J., ... Cox, P. M. (2011, September). The Joint UK Land Environment Simulator (JULES), model description – Part 2: Carbon fluxes and vegetation dynamics. *Geoscientific Model Development*, *4*(3), 701–722. Retrieved 2021-04-14, from https://gmd.copernicus.org/articles/4/701/2011/ doi: 10.5194/gmd-4-701-2011

Coleman, K., & Jenkinson, D. S. (1996). RothC-26.3 - A Model for the turnover of carbon in soil. In D. S. Powlson, P. Smith, & J. U. Smith (Eds.), *Evaluation of Soil Organic Matter Models* (pp. 237–246). Berlin, Heidelberg: Springer Berlin Heidelberg. Retrieved 2021-03-24, from http://link.springer.com/10.1007/978-3-642-61094-3_17 doi: 10.1007/978-3-642-61094-3_17

Crowther, T. W., Van Den Hoogen, J., Wan, J., Mayes, M. A., Keiser, A. D., Mo, L., ... Maynard, D. S. (2019, August). The global soil community and its influence on biogeochemistry. *Science*, *365*(6455), eaav0550. Retrieved 2023-09-20, from https://www.science.org/doi/10.1126/science.aav0550 doi: 10.1126/science.aav0550

Danabasoglu, G., Lamarque, J., Bacmeister, J., Bailey, D. A., DuVivier, A. K., Edwards, J., ... Strand, W. G. (2020, February). The Community Earth System Model Version 2 (CESM2). *Journal of Advances in Modeling Earth Systems*, *12*(2). Retrieved 2021-04-22, from https://onlinelibrary.wiley.com/doi/10.1029/2019MS001916 doi: 10.1029/2019MS001916

Doetterl, S., Stevens, A., Six, J., Merckx, R., Van Oost, K., Casanova Pinto, M., ... Boeckx, P. (2015, October). Soil carbon storage controlled by interactions between geochemistry and climate. *Nature Geoscience*, *8*(10), 780–783. Retrieved 2021-04-21, from http://www.nature.com/articles/ngeo2516 doi: 10.1038/ngeo2516

Dungait, J. A. J., Hopkins, D. W., Gregory, A. S., & Whitmore, A. P. (2012, June). Soil organic matter turnover is governed by accessibility not recalcitrance. *Global Change Biology*, *18*(6), 1781–1796. Retrieved 2021-04-21, from http://doi.wiley.com/10.1111/j.1365-2486.2012.02665.x doi: 10.1111/j.1365-2486.2012.02665.x

Eckmeier, E., Van der Borg, K., Tegtmeier, U., Schmidt, M. W. I., & Gerlach, R. (2009). Dating Charred Soil Organic Matter: Comparison of Radiocarbon Ages from Macrocharcoals and Chemically Separated Charcoal Carbon. *Radiocarbon*, *51*(2), 437–443. Retrieved 2022-02-07, from https://www.cambridge.org/core/product/identifier/S0033822200055831/type/journal_article doi: 10.1017/S0033822200055831

Fan, X., Gao, D., Zhao, C., Wang, C., Qu, Y., Zhang, J., & Bai, E. (2021, August). Improved model simulation of soil carbon cycling by representing the microbially derived organic carbon pool. *The ISME Journal*, *15*(8), 2248–2263. Retrieved 2022-07-10, from http://www.nature.com/articles/s41396-021-00914-0 doi: 10.1038/s41396-021-00914-0

Friedlingstein, P., Meinshausen, M., Arora, V. K., Jones, C. D., Anav, A., Liddicoat, S. K., & Knutti, R. (2014, January). Uncertainties in CMIP5 Climate Projections due to Carbon Cycle Feedbacks. *Journal of Climate*, *27*(2), 511–526. Retrieved 2022-09-19, from http://journals.ametsoc.org/doi/10.1175/JCLI-D-12-00579.1 doi: 10.1175/JCLI-D-12-00579.1

Friedlingstein, P., O'Sullivan, M., Jones, M. W., Andrew, R. M., Gregor, L., Hauck, J., ... Zheng, B. (2022, November). Global Carbon Budget 2022. *Earth System Science Data*, *14*(11), 4811–4900. Retrieved 2023-07-18, from https://essd.copernicus.org/articles/14/4811/2022/ doi: 10.5194/essd-14-4811-2022

Gaudinski, J. B., Trumbore, S. E., Davidson, E. A., & Zheng, S. (2000). Soil carbon cycling in a temperate forest: radiocarbon-based estimates of residence times, sequestration rates and partitioning of fluxes. *Biogeochemistry*, *51*(1), 33–69. Retrieved 2022-05-04, from http://link.springer.com/10.1023/A:1006301010014 doi: 10.1023/A:1006301010014

German, D. P., Marcelo, K. R. B., Stone, M. M., & Allison, S. D. (2012, April). The Michaelis-Menten kinetics of soil extracellular enzymes in response to temperature: a cross-latitudinal study. *Global Change Biology*, *18*(4), 1468–1479. Retrieved 2021-04-19, from http://doi.wiley.com/10.1111/j.1365-2486.2011.02615.x doi: 10.1111/j.1365-2486.2011.02615.x

Golchin, A., Oades, J., Skjemstad, J., & Clarke, P. (1994). Study of free and occluded particulate organic matter in soils by solid state ^{13}C CP/MAS NMR spectroscopy and scanning electron microscopy. *Soil Research*, *32*(2), 285. Retrieved 2023-07-01, from http://www.publish.csiro.au/?paper=SR9940285 doi: 10.1071/SR9940285

Graven, H., Allison, C. E., Etheridge, D. M., Hammer, S., Keeling, R. F., Levin, I., ... White, J. W. C. (2017, December). Compiled records of carbon isotopes in atmospheric CO_2 for historical simulations in CMIP6. *Geoscientific Model Development*, *10*(12), 4405–4417. Retrieved 2021-03-10, from https://gmd.copernicus.org/articles/10/4405/2017/ doi: 10.5194/gmd-10-4405-2017

Graven, H., Keeling, R. F., & Rogelj, J. (2020, November). Changes to Carbon Isotopes in Atmospheric CO_2 Over the Industrial Era and Into the Future. *Global Biogeochemical Cycles*, *34*(11). Retrieved 2023-08-02, from https://onlinelibrary.wiley.com/doi/10.1029/2019GB006170 doi: 10.1029/2019GB006170

Griepentrog, M., Bodé, S., Boeckx, P., Hagedorn, F., Heim, A., & Schmidt, M. W. I. (2014, January). Nitrogen deposition promotes the production of new fungal residues but retards the decomposition of old residues in forest soil fractions. *Global Change Biology*, *20*(1), 327–340. Retrieved 2022-02-11, from https://onlinelibrary.wiley.com/doi/10.1111/gcb.12374 doi: 10.1111/gcb.12374

Griepentrog, M., Eglinton, T. I., Hagedorn, F., Schmidt, M. W. I., & Wiesenberg, G. L. B. (2015, January). Interactive effects of elevated CO_2 and nitrogen deposition on fatty acid molecular and isotope composition of above- and belowground tree biomass and forest soil fractions. *Global Change Biology*, *21*(1), 473–486. Retrieved 2021-09-26, from https://onlinelibrary.wiley.com/doi/10.1111/gcb.12666 doi: 10.1111/gcb.12666

Hajdas, I., Schlumpf, N., Minikus-Stary, N., Hagedorn, F., Eckmeier, E., Schoch, W., ... Cherubini, P. (2007, June). Radiocarbon ages of soil charcoals from the southern Alps, Ticino, Switzerland. *Nuclear Instruments and Methods in Physics Research Section B: Beam Interactions with Materials and Atoms*, *259*(1), 398–402. Retrieved 2023-08-28, from https://linkinghub.elsevier.com/retrieve/pii/S0168583X07004028 doi: 10.1016/j.nimb.2007.02.075

Harden, J. W., Fries, T. L., & Pavich, M. J. (2002). Cycling of Beryllium and Carbon through hillslope soils in Iowa. *Biogeochemistry*, *60*, 317–336. doi: 10.1023/A:1020308729553

He, Y., Trumbore, S. E., Torn, M. S., Harden, J. W., Vaughn, L. J. S., Allison, S. D., & Randerson, J. T. (2016, September). Radiocarbon constraints imply reduced carbon uptake by soils during the 21st century. *Science*, *353*(6306), 1419–1424. Retrieved 2022-05-28, from https://www.sciencemag.org/lookup/doi/10.1126/science.aad4273 doi: 10.1126/science.aad4273

Heckman, K. (2010). *Pedogenesis & Carbon Dynamics Across A Lithosequence Under Ponderosa Pine* (Doctoral dissertation). Retrieved 2023-10-06, from https://zenodo.org/record/1486081 (Publisher: Zenodo)

Heckman, K., Lawrence, C. R., & Harden, J. W. (2018, February). A sequential selective dissolution method to quantify storage and stability of organic carbon associated with Al and Fe hydroxide phases. *Geoderma*, *312*, 24–35. Retrieved 2023-07-01, from https://linkinghub.elsevier.com/retrieve/pii/S0016706117312703 doi: 10.1016/j.geoderma.2017.09.043

Hicks Pries, C. E., Castanha, C., Porras, R. C., & Torn, M. S. (2017, March). The whole-soil carbon flux in response to warming. *Science*, *355*(6332), 1420–1423. Retrieved 2022-07-10, from https://www.science.org/doi/10.1126/science.aal1319 doi: 10.1126/science.aal1319

Hicks Pries, C. E., Sulman, B. N., West, C., O'Neill, C., Poppleton, E., Porras, R. C., … Torn, M. S. (2018, October). Root litter decomposition slows with soil depth. *Soil Biology and Biochemistry*, *125*, 103–114. Retrieved 2022-07-26, from https://linkinghub.elsevier.com/retrieve/pii/S003807171830230X doi: 10.1016/j.soilbio.2018.07.002

Jagadamma, S., Lal, R., Ussiri, D. A. N., Trumbore, S. E., & Mestelan, S. (2010, April). Evaluation of structural chemistry and isotopic signatures of refractory soil organic carbon fraction isolated by wet oxidation methods. *Biogeochemistry*, *98*(1-3), 29–44. Retrieved 2023-08-28, from http://link.springer.com/10.1007/s10533-009-9374-0 doi: 10.1007/s10533-009-9374-0

Kleber, M., Nico, P. S., Plante, A., Filley, T., Kramer, M., Swanston, C., & Sollins, P. (2011, February). Old and stable soil organic matter is not necessarily chemically recalcitrant: implications for modeling concepts and temperature sensitivity: SLOW TURNOVER OF LABILE SOIL ORGANIC MATTER. *Global Change Biology*, *17*(2), 1097–1107. Retrieved 2022-01-28, from https://onlinelibrary.wiley.com/doi/10.1111/j.1365-2486.2010.02278.x doi: 10.1111/j.1365-2486.2010.02278.x

Kyker-Snowman, E., Wieder, W. R., Frey, S. D., & Grandy, A. S. (2020, September). Stoichiometrically coupled carbon and nitrogen cycling in the MIcrobial-MIneral Carbon Stabilization model version 1.0 (MIMICS-CN v1.0). *Geoscientific Model Development*, *13*(9), 4413–4434. Retrieved 2023-06-29, from https://gmd.copernicus.org/articles/13/4413/2020/ doi: 10.5194/gmd-13-4413-2020

Lavallee, J. M., Soong, J. L., & Cotrufo, M. F. (2020, January). Conceptualizing soil organic matter into particulate and mineral-associated forms to address global change in the 21st century. *Global Change Biology*, *26*(1), 261–273. Retrieved 2021-12-08, from https://onlinelibrary.wiley.com/doi/10.1111/gcb.14859 doi: 10.1111/gcb.14859

Lawrence, C. R., Beem-Miller, J., Hoyt, A. M., Monroe, G., Sierra, C. A., Stoner, S., … Wagai, R. (2020, January). An open-source database for the synthesis of soil radiocarbon data: International Soil Radiocarbon Database (ISRaD) version 1.0. *Earth System Science Data*, *12*(1), 61–76. Retrieved 2022-07-10, from https://essd.copernicus.org/articles/12/61/2020/ doi: 10.5194/essd-12-61-2020

Lehmann, J., & Kleber, M. (2015, December). The contentious nature of soil organic matter. *Nature*, *528*(7580), 60–68. Retrieved 2021-04-21, from http://www.nature.com/articles/nature16069 doi: 10.1038/nature16069

Leifeld, J. (2008, May). Biased 14C-derived organic carbon turnover estimates following black carbon input to soil: an exploration with RothC. *Biogeochemistry*, *88*(3), 205–211. Retrieved 2023-08-28, from http://link.springer.com/10.1007/s10533-008-9209-4 doi: 10.1007/s10533-008-9209-4

Leifeld, J., Zimmermann, M., & Fuhrer, J. (2008, December). Simulating decomposition of labile soil organic carbon: Effects of pH. *Soil Biol-*

ogy and Biochemistry, *40*(12), 2948–2951. Retrieved 2023-08-28, from https://linkinghub.elsevier.com/retrieve/pii/S0038071708002861 doi: 10.1016/j.soilbio.2008.08.019

Leifeld, J., Zimmermann, M., Fuhrer, J., & Conen, F. (2009, March). Storage and turnover of carbon in grassland soils along an elevation gradient in the Swiss Alps. *Global Change Biology*, *15*(3), 668–679. Retrieved 2023-04-07, from https://onlinelibrary.wiley.com/doi/10.1111/j.1365-2486.2008.01782.x doi: 10.1111/j.1365-2486.2008.01782.x

Liu, K., Xu, Y., Feng, W., Zhang, X., Yao, S., & Zhang, B. (2020, December). Modeling the dynamics of protected and primed organic carbon in soil and aggregates under constant soil moisture following litter incorporation. *Soil Biology and Biochemistry*, *151*, 108039. Retrieved 2022-07-10, from https://linkinghub.elsevier.com/retrieve/pii/S0038071720303357 doi: 10.1016/j.soilbio.2020.108039

Lybrand, R. A., Heckman, K., & Rasmussen, C. (2017, August). Soil organic carbon partitioning and ^{14}C variation in desert and conifer ecosystems of southern Arizona. *Biogeochemistry*, *134*(3), 261–277. Retrieved 2023-07-01, from http://link.springer.com/10.1007/s10533-017-0360-7 doi: 10.1007/s10533-017-0360-7

Malamoud, K., McBratney, A. B., Minasny, B., & Field, D. J. (2009, February). Modelling how carbon affects soil structure. *Geoderma*, *149*(1-2), 19–26. Retrieved 2022-07-10, from https://linkinghub.elsevier.com/retrieve/pii/S0016706108003169 doi: 10.1016/j.geoderma.2008.10.018

Marín-Spiotta, E., Swanston, C. W., Torn, M. S., Silver, W. L., & Burton, S. D. (2008, January). Chemical and mineral control of soil carbon turnover in abandoned tropical pastures. *Geoderma*, *143*(1-2), 49–62. Retrieved 2023-07-01, from https://linkinghub.elsevier.com/retrieve/pii/S0016706107002807 doi: 10.1016/j.geoderma.2007.10.001

McFarlane, K. J., Torn, M. S., Hanson, P. J., Porras, R. C., Swanston, C. W., Callaham, M. A., & Guilderson, T. P. (2013, March). Comparison of soil organic matter dynamics at five temperate deciduous forests with physical fractionation and radiocarbon measurements. *Biogeochemistry*, *112*(1-3), 457–476. Retrieved 2023-07-01, from http://link.springer.com/10.1007/s10533-012-9740-1 doi: 10.1007/s10533-012-9740-1

Meyer, S., Leifeld, J., Bahn, M., & Fuhrer, J. (2012, February). Free and protected soil organic carbon dynamics respond differently to abandonment of mountain grassland. *Biogeosciences*, *9*(2), 853–865. Retrieved 2023-10-06, from https://bg.copernicus.org/articles/9/853/2012/ doi: 10.5194/bg-9-853-2012

Mikutta, R., Turner, S., Schippers, A., Gentsch, N., Meyer-Stüve, S., Condron, L. M., … Guggenberger, G. (2019, July). Microbial and abiotic controls on mineral-associated organic matter in soil profiles along an ecosystem gradient. *Scientific Reports*, *9*(1), 10294. Retrieved 2023-08-28, from https://www.nature.com/articles/s41598-019-46501-4 doi: 10.1038/s41598-019-46501-4

Moore, J. A. M., Sulman, B. N., Mayes, M. A., Patterson, C. M., & Classen, A. T. (2020, April). Plant roots stimulate the decomposition of complex, but not simple, soil carbon. *Functional Ecology*, *34*(4), 899–910. Retrieved 2022-08-29, from https://onlinelibrary.wiley.com/doi/10.1111/1365-2435.13510 doi: 10.1111/1365-2435.13510

Parton, W. J., Schimel, D. S., Cole, C. V., & Ojima, D. S. (1987, September). Analysis of Factors Controlling Soil Organic Matter Levels in Great Plains Grasslands. *Soil Science Society of America Journal*, *51*(5), 1173–1179. Retrieved 2023-07-18, from http://doi.wiley.com/10.2136/sssaj1987.03615995005100050015x doi: 10.2136/sssaj1987.03615995005100050015x

Poeplau, C., Don, A., Six, J., Kaiser, M., Benbi, D., Chenu, C., ... Nieder, R. (2018, October). Isolating organic carbon fractions with varying turnover rates in temperate agricultural soils – A comprehensive method comparison. *Soil Biology and Biochemistry*, *125*, 10–26. Retrieved 2022-07-10, from `https://linkinghub.elsevier.com/retrieve/pii/S0038071718302232` doi: 10.1016/j.soilbio.2018.06.025

Poggio, L., de Sousa, L. M., Batjes, N. H., Heuvelink, G. B. M., Kempen, B., Ribeiro, E., & Rossiter, D. (2021, June). SoilGrids 2.0: producing soil information for the globe with quantified spatial uncertainty. *SOIL*, *7*(1), 217–240. Retrieved 2022-09-25, from `https://soil.copernicus.org/articles/7/217/2021/` doi: 10.5194/soil-7-217-2021

Rahman, M. M., Tsukamoto, J., Rahman, M. M., Yoneyama, A., & Mostafa, K. M. (2013, August). Lignin and its effects on litter decomposition in forest ecosystems. *Chemistry and Ecology*, *29*(6), 540–553. Retrieved 2023-11-25, from `http://www.tandfonline.com/doi/abs/10.1080/02757540.2013.790380` doi: 10.1080/02757540.2013.790380

Rasmussen, C., Heckman, K., Wieder, W. R., Keiluweit, M., Lawrence, C. R., Berhe, A. A., ... Wagai, R. (2018, February). Beyond clay: towards an improved set of variables for predicting soil organic matter content. *Biogeochemistry*, *137*(3), 297–306. Retrieved 2023-09-25, from `http://link.springer.com/10.1007/s10533-018-0424-3` doi: 10.1007/s10533-018-0424-3

Rasmussen, C., Throckmorton, H., Liles, G., Heckman, K., Meding, S., & Horwath, W. (2018, July). Controls on Soil Organic Carbon Partitioning and Stabilization in the California Sierra Nevada. *Soil Systems*, *2*(3), 41. Retrieved 2023-07-02, from `http://www.mdpi.com/2571-8789/2/3/41` doi: 10.3390/soilsystems2030041

Roberts, M. L., & Southon, J. R. (2007). A Preliminary Determination of the Absolute $^{14}C/^{12}C$ Ratio of OX-I. *Radiocarbon*, *49*(2), 441–445. Retrieved 2021-04-11, from `https://www.cambridge.org/core/product/identifier/S0033822200042363/type/journal_article` doi: 10.1017/S0033822200042363

Robertson, A. D., Paustian, K., Ogle, S., Wallenstein, M. D., Lugato, E., & Cotrufo, M. F. (2019, March). Unifying soil organic matter formation and persistence frameworks: the MEMS model. *Biogeosciences*, *16*(6), 1225–1248. Retrieved 2022-01-28, from `https://bg.copernicus.org/articles/16/1225/2019/` doi: 10.5194/bg-16-1225-2019

Rodgers, K. B., Lee, S.-S., Rosenbloom, N., Timmermann, A., Danabasoglu, G., Deser, C., ... Yeager, S. G. (2021, December). Ubiquity of human-induced changes in climate variability. *Earth System Dynamics*, *12*(4), 1393–1411. Retrieved 2022-09-25, from `https://esd.copernicus.org/articles/12/1393/2021/` doi: 10.5194/esd-12-1393-2021

Rowley, M. C., Grand, S., & Verrecchia, E. P. (2018, January). Calcium-mediated stabilisation of soil organic carbon. *Biogeochemistry*, *137*(1-2), 27–49. Retrieved 2023-09-25, from `http://link.springer.com/10.1007/s10533-017-0410-1` doi: 10.1007/s10533-017-0410-1

Salazar, A., Sulman, B. N., & Dukes, J. S. (2018, January). Microbial dormancy promotes microbial biomass and respiration across pulses of drying-wetting stress. *Soil Biology and Biochemistry*, *116*, 237–244. Retrieved 2023-06-25, from `https://linkinghub.elsevier.com/retrieve/pii/S0038071717306120` doi: 10.1016/j.soilbio.2017.10.017

Schimel, J. (2023, March). Modeling ecosystem-scale carbon dynamics in soil: The microbial dimension. *Soil Biology and Biochemistry*, *178*, 108948. Retrieved 2023-11-18, from `https://linkinghub.elsevier.com/retrieve/pii/S003807172300010X` doi: 10.1016/j.soilbio.2023.108948

Schmidt, M. W. I., Torn, M. S., Abiven, S., Dittmar, T., Guggenberger, G., Janssens, I. A., ... Trumbore, S. E. (2011, October). Persistence of soil organic matter as an ecosystem property. *Nature*, *478*(7367), 49–56. Retrieved 2022-02-11, from http://www.nature.com/articles/nature10386 doi: 10.1038/nature10386

Schrumpf, M., & Kaiser, K. (2015, February). Large differences in estimates of soil organic carbon turnover in density fractions by using single and repeated radiocarbon inventories. *Geoderma*, *239-240*, 168–178. Retrieved 2022-02-06, from https://linkinghub.elsevier.com/retrieve/pii/S0016706114003577 doi: 10.1016/j.geoderma.2014.09.025

Schrumpf, M., Kaiser, K., Guggenberger, G., Persson, T., Kögel-Knabner, I., & Schulze, E.-D. (2013, March). Storage and stability of organic carbon in soils as related to depth, occlusion within aggregates, and attachment to minerals. *Biogeosciences*, *10*(3), 1675–1691. Retrieved 2023-07-02, from https://bg.copernicus.org/articles/10/1675/2013/ doi: 10.5194/bg-10-1675-2013

Schrumpf, M., Kaiser, K., Mayer, A., Hempel, G., & Trumbore, S. (2021, February). Age distribution, extractability, and stability of mineral-bound organic carbon in central European soils. *Biogeosciences*, *18*(3), 1241–1257. Retrieved 2023-08-28, from https://bg.copernicus.org/articles/18/1241/2021/ doi: 10.5194/bg-18-1241-2021

Segoli, M., De Gryze, S., Dou, F., Lee, J., Post, W., Denef, K., & Six, J. (2013, August). AggModel: A soil organic matter model with measurable pools for use in incubation studies. *Ecological Modelling*, *263*, 1–9. Retrieved 2021-04-21, from https://linkinghub.elsevier.com/retrieve/pii/S0304380013002147 doi: 10.1016/j.ecolmodel.2013.04.010

Sierra, C. A., Trumbore, S. E., Davidson, E. A., Vicca, S., & Janssens, I. (2015, March). Sensitivity of decomposition rates of soil organic matter with respect to simultaneous changes in temperature and moisture. *Journal of Advances in Modeling Earth Systems*, *7*(1), 335–356. Retrieved 2021-04-19, from http://doi.wiley.com/10.1002/2014MS000358 doi: 10.1002/2014MS000358

Soucémarianadin, L., Reisser, M., Cécillon, L., Barré, P., Nicolas, M., & Abiven, S. (2019, June). Pyrogenic carbon content and dynamics in top and subsoil of French forests. *Soil Biology and Biochemistry*, *133*, 12–15. Retrieved 2023-08-28, from https://linkinghub.elsevier.com/retrieve/pii/S0038071719300537 doi: 10.1016/j.soilbio.2019.02.013

Stamati, F. E., Nikolaidis, N. P., Banwart, S., & Blum, W. E. (2013, December). A coupled carbon, aggregation, and structure turnover (CAST) model for topsoils. *Geoderma*, *211-212*, 51–64. Retrieved 2022-05-29, from https://linkinghub.elsevier.com/retrieve/pii/S0016706113002140 doi: 10.1016/j.geoderma.2013.06.014

Stoner, S. W., Schrumpf, M., Hoyt, A., Sierra, C. A., Doetterl, S., Galy, V., & Trumbore, S. (2023, August). How well does ramped thermal oxidation quantify the age distribution of soil carbon? Assessing thermal stability of physically and chemically fractionated soil organic matter. *Biogeosciences*, *20*(15), 3151–3163. Retrieved 2023-08-26, from https://bg.copernicus.org/articles/20/3151/2023/ doi: 10.5194/bg-20-3151-2023

Sulman, B. N., Brzostek, E. R., Medici, C., Shevliakova, E., Menge, D. N. L., & Phillips, R. P. (2017, August). Feedbacks between plant N demand and rhizosphere priming depend on type of mycorrhizal association. *Ecology Letters*, *20*(8), 1043–1053. Retrieved 2022-07-26, from https://onlinelibrary.wiley.com/doi/10.1111/ele.12802 doi: 10.1111/ele.12802

Sulman, B. N., Phillips, R. P., Oishi, A. C., Shevliakova, E., & Pacala, S. W. (2014, December). Microbe-driven turnover offsets mineral-mediated storage of soil carbon under elevated CO2. *Nature Climate Change*, *4*(12), 1099–1102. Retrieved 2022-05-29, from http://www.nature.com/articles/nclimate2436 doi: 10.1038/nclimate2436

Tian, H., Yang, J., Lu, C., Xu, R., Canadell, J. G., Jackson, R. B., . . . Zhu, Q. (2018, June). The Global N2O Model Intercomparison Project. *Bulletin of the American Meteorological Society*, *99*(6), 1231–1251. Retrieved 2023-06-20, from https://journals.ametsoc.org/view/journals/bams/99/6/bams-d-17-0212.1.xml doi: 10.1175/BAMS-D-17-0212.1

Tipping, E., & Rowe, E. C. (2019, March). Modelling the physical states, element stoichiometries and residence times of topsoil organic matter. *European Journal of Soil Science*, *70*(2), 321–337. Retrieved 2022-07-10, from https://onlinelibrary.wiley.com/doi/10.1111/ejss.12785 doi: 10.1111/ejss.12785

Trumbore, S. E., Sierra, C. A., & Hicks Pries, C. E. (2016). Radiocarbon Nomenclature, Theory, Models, and Interpretation: Measuring Age, Determining Cycling Rates, and Tracing Source Pools. In E. A. Schuur, E. Druffel, & S. E. Trumbore (Eds.), *Radiocarbon and Climate Change* (pp. 45–82). Cham: Springer International Publishing. Retrieved 2021-04-05, from http://link.springer.com/10.1007/978-3-319-25643-6_3 doi: 10.1007/978-3-319-25643-6_3

van der Voort, T. S., Mannu, U., Hagedorn, F., McIntyre, C., Walthert, L., Schleppi, P., . . . Eglinton, T. I. (2019, August). Dynamics of deep soil carbon – insights from ^{14}C time series across a climatic gradient. *Biogeosciences*, *16*(16), 3233–3246. Retrieved 2021-03-21, from https://bg.copernicus.org/articles/16/3233/2019/ doi: 10.5194/bg-16-3233-2019

van der Voort, T. S., Zell, C. I., Hagedorn, F., Feng, X., McIntyre, C. P., Haghipour, N., . . . Eglinton, T. I. (2017, December). Diverse Soil Carbon Dynamics Expressed at the Molecular Level: Molecular Level Soil Carbon Dynamics. *Geophysical Research Letters*, *44*(23), 11,840–11,850. Retrieved 2021-03-21, from http://doi.wiley.com/10.1002/2017GL076188 doi: 10.1002/2017GL076188

Vogel, C., Mueller, C. W., Höschen, C., Buegger, F., Heister, K., Schulz, S., . . . Kögel-Knabner, I. (2014, January). Submicron structures provide preferential spots for carbon and nitrogen sequestration in soils. *Nature Communications*, *5*(1), 2947. Retrieved 2023-09-20, from https://www.nature.com/articles/ncomms3947 doi: 10.1038/ncomms3947

von Lützow, M., Kögel-Knabner, I., Ekschmitt, K., Flessa, H., Guggenberger, G., Matzner, E., & Marschner, B. (2007, September). SOM fractionation methods: Relevance to functional pools and to stabilization mechanisms. *Soil Biology and Biochemistry*, *39*(9), 2183–2207. Retrieved 2022-01-26, from https://linkinghub.elsevier.com/retrieve/pii/S0038071707001125 doi: 10.1016/j.soilbio.2007.03.007

Wagai, R., Mayer, L. M., & Kitayama, K. (2009, February). Nature of the "occluded" low-density fraction in soil organic matter studies: A critical review. *Soil Science and Plant Nutrition*, *55*(1), 13–25. Retrieved 2022-05-29, from http://www.tandfonline.com/doi/abs/10.1111/j.1747-0765.2008.00356.x doi: 10.1111/j.1747-0765.2008.00356.x

Wang, G., Gao, Q., Yang, Y., Hobbie, S. E., Reich, P. B., & Zhou, J. (2022, March). Soil enzymes as indicators of soil function: A step toward greater realism in microbial ecological modeling. *Global Change Biology*, *28*(5), 1935–1950. Retrieved 2023-06-23, from https://onlinelibrary.wiley.com/doi/10.1111/gcb.16036 doi: 10.1111/gcb.16036

Wang, G., Jagadamma, S., Mayes, M. A., Schadt, C. W., Megan Steinweg, J., Gu, L., & Post, W. M. (2015, January). Microbial dormancy improves development and experimental validation of ecosystem model. *The ISME Journal*, *9*(1), 226–237. Retrieved 2021-04-21, from http://www.nature.com/articles/

ismej2014120 doi: 10.1038/ismej.2014.120

Wang, G., Post, W. M., & Mayes, M. A. (2013, January). Development of microbial-enzyme-mediated decomposition model parameters through steady-state and dynamic analyses. *Ecological Applications*, *23*(1), 255–272. Retrieved 2021-04-21, from http://doi.wiley.com/10.1890/12-0681.1 doi: 10.1890/12-0681.1

Wang, Y., Zhang, H., Ciais, P., Goll, D., Huang, Y., Wood, J. D., ... Prescher, A. (2021, April). Microbial Activity and Root Carbon Inputs Are More Important than Soil Carbon Diffusion in Simulating Soil Carbon Profiles. *Journal of Geophysical Research: Biogeosciences*, *126*(4). Retrieved 2022-07-10, from https://onlinelibrary.wiley.com/doi/10.1029/2020JG006205 doi: 10.1029/2020JG006205

Wieder, W. R., Grandy, A. S., Kallenbach, C. M., & Bonan, G. B. (2014, July). Integrating microbial physiology and physio-chemical principles in soils with the MIcrobial-MIneral Carbon Stabilization (MIMICS) model. *Biogeosciences*, *11*(14), 3899–3917. Retrieved 2021-05-25, from https://bg.copernicus.org/articles/11/3899/2014/ doi: 10.5194/bg-11-3899-2014

Wieder, W. R., Grandy, A. S., Kallenbach, C. M., Taylor, P. G., & Bonan, G. B. (2015, June). Representing life in the Earth system with soil microbial functional traits in the MIMICS model. *Geoscientific Model Development*, *8*(6), 1789–1808. Retrieved 2023-06-29, from https://gmd.copernicus.org/articles/8/1789/2015/ doi: 10.5194/gmd-8-1789-2015

Woolf, D., & Lehmann, J. (2019, December). Microbial models with minimal mineral protection can explain long-term soil organic carbon persistence. *Scientific Reports*, *9*(1), 6522. Retrieved 2021-10-01, from http://www.nature.com/articles/s41598-019-43026-8 doi: 10.1038/s41598-019-43026-8

Xiao, L., Wang, G., Chang, J., Chen, Y., Guo, X., Mao, X., ... Luo, Z. (2023, August). Global depth distribution of belowground net primary productivity and its drivers. *Global Ecology and Biogeography*, *32*(8), 1435–1451. Retrieved 2023-07-16, from https://onlinelibrary.wiley.com/doi/10.1111/geb.13705 doi: 10.1111/geb.13705

Yu, L., Ahrens, B., Wutzler, T., Schrumpf, M., & Zaehle, S. (2020, February). Jena Soil Model (JSM v1.0; revision 1934): a microbial soil organic carbon model integrated with nitrogen and phosphorus processes. *Geoscientific Model Development*, *13*(2), 783–803. Retrieved 2022-07-10, from https://gmd.copernicus.org/articles/13/783/2020/ doi: 10.5194/gmd-13-783-2020

Zhang, H., Goll, D. S., Wang, Y., Ciais, P., Wieder, W. R., Abramoff, R., ... Tang, X. (2020, April). Microbial dynamics and soil physicochemical properties explain large-scale variations in soil organic carbon. *Global Change Biology*, *26*(4), 2668–2685. Retrieved 2022-07-10, from https://onlinelibrary.wiley.com/doi/10.1111/gcb.14994 doi: 10.1111/gcb.14994

Zhang, Y., Lavallee, J. M., Robertson, A. D., Even, R., Ogle, S. M., Paustian, K., & Cotrufo, M. F. (2021, May). Simulating measurable ecosystem carbon and nitrogen dynamics with the mechanistically defined MEMS 2.0 model. *Biogeosciences*, *18*(10), 3147–3171. Retrieved 2022-07-10, from https://bg.copernicus.org/articles/18/3147/2021/ doi: 10.5194/bg-18-3147-2021

Supporting Information for "Radiocarbon analysis reveals underestimation of soil organic carbon persistence in new-generation soil models"

Alexander S. Brunmayr[1], Frank Hagedorn[2], Margaux Moreno Duborgel[2,3],

Luisa I. Minich[2,3], Heather D. Graven[1]

[1]Imperial College London, Department of Physics

[2]Eidgenössische Forschungsanstalt WSL

[3]ETH Zurich, Department of Earth Sciences

Contents of this file

1. Text S1 to S5

2. Figures S1 to S12

3. Table S1

Introduction

This document provides further information on the specific model versions and implementations used in this study (section S1, Figures S1-S5), and specifies which simulated pools were associated to which measured soil fraction (section S2, Table S1). It also explains how we re-implemented non-isotopic models with ^{14}C (section S3), and why the ^{14}C implementation of SOMic and the newest version of MIMICS are incorrect (section S4, Figures S6-S7). Section S5 gives some more details on Millennial's turnover times. Finally, Figures S8-S12 at the end of this document show plots of model predictions against observations for each model.

S1. Further information on model versions and implementations

The source codes of all the selected model versions are openly available. By having direct access to the code with which the model developers produced their results, we can be more confident that we test an implementation of the models as intended by their respective authors.

Our final implementations of the Millennial, CORPSE, and MIMICS models are available as python modules on our GitHub repository `https://github.com/asb219/evaluate-SOC-models`. Our slightly modified implementation of the MEND model in `https://github.com/asb219/MEND` is added to our repository as a git submodule. Finally, we installed the SOMic model's R package directly from our forked `https://github.com/asb219/somic1` GitHub repository.

S1.1. Millennial

We use Millennial V2 with Michaelis-Menten kinetics as described in Abramoff et al. (2022). We re-implemented the model with ^{14}C in Python based on the original R code in the `https://github.com/rabramoff/Millennial` repository under the tag "v2" (commit `e95bca9` from September 2021). We used the model equations from file `R/models/derivs_V2_MM.R` in the repository and ran the model with the fitted parameter values from the file `Fortran/MillennialV2/simulationv2/soilpara_in_fit.txt` in the repository. The initial condition for both carbon and ^{14}C stocks is found by first solving for a pre-industrial steady state, similarly to the model tutorial `R/simulation/model_tutorial.Rmd` in the repository, and then running the model from steady state for 200 years using time-varying pre-industrial forcing data featuring a seasonal cycle. The final state of that spinup is then used as the initial condition for the final run of the model over the 1850-2014 period. The model runs with daily time steps, and though the model tutorial uses the 4th order Runge-Kutta integration method, we integrate the equations simply with the forward Euler method, which is stable and precise enough with daily time steps.

S1.2. CORPSE

The CORPSE model was originally described in Sulman, Phillips, Oishi, Shevliakova, and Pacala (2014). There are currently at least six publicly available versions of CORPSE. Since we are mostly interested in carbon dynamics, the lead developer Benjamin Sulman recommended we use the most up-to-date carbon-only implementation in `https://github.com/bsulman/CORPSE-fire-response` (latest commit at time of writing: `19ee2c7` from February 2021). We reimplemented CORPSE with ^{14}C based on the equations in file `CORPSE_array.py` and using the parameter values from file `Whitman_sims.py` in that repository. However, the equation for the clay-related rate modifying factor is taken from file `code/CORPSE_integrate.py` in repository `https://github.com/bsulman/CORPSE-N`, since the model seems to be working more reliably with that version of the equation. Like in Millennial, the initial condition is found by solving for a pre-industrial steady state and spinning up for 200 years from that steady state. If the solver is unable to find a steady state, the model is spun up for 4000 years. The model runs with daily time steps and uses the forward Euler integration method.

S1.3. SOMic

We use version 1.0 of the SOMic model as described in (Woolf & Lehmann, 2019). The original code is available on the GitHub repository `https://github.com/domwoolf/`

`somic1` (hash of latest commit at time of writing: `be34e56` from June 2019). However, we forked the repository to `https://github.com/asb219/somic1` in order to fix a minor issue in its ^{14}C implementation (see reason in section S4.1), and used the version released under the tag "v1.1-asb219" to produce our results. We spin up the model for 5000 years to get the initial carbon and ^{14}C stocks. The model runs with monthly time steps and uses the forward Euler integration method.

S1.4. MEND

We use the latest version of the default MEND model with carbon-nitrogen coupling as described in G. Wang et al. (2022). Our ^{14}C re-implementation is based on the code from commit `92323c7` (from February 2022) of the GitHub repository `https://github.com/wanggangsheng/MEND`. We forked the repository from that commit to `https://github.com/asb219/MEND` so we could adapt the model input and output to our purposes. We use all the default model settings and the optimized parameter values provided in the Fortran namelist file `MEND_namelist.nml` in the repository. The pre-industrial soil carbon and nitrogen stocks are found by initializing the model with the default initial state from file `userio/inp/SOIL_ini.dat` and spinning up for 400 year with pre-industrial forcing data. The pre-industrial soil ^{14}C levels are found by running the spun-up model for another 1000 years with pre-industrial forcing data. The model runs with hourly time steps and uses the forward Euler integration method.

S1.5. MIMICS

We use the MIMICS-CN v1.0 model, as published in (Kyker-Snowman et al., 2020), because the latest version of MIMICS (Y. Wang et al., 2021) did not correctly implement ^{14}C (see section SS4.2). The original R code of MIMICS-CN v1.0 is available on `https://zenodo.org/records/3534562`. It already implements stable isotope tracers, but no radioactive isotopes such as ^{14}C, so we re-implemented the model with ^{14}C in python. Like for Millennial and CORPSE, we spin up for 200 years from the pre-industrial steady-state solution. If no steady state can be found, we spin up for 4000 years. The model runs with hourly time steps and uses the forward Euler integration method.

S2. Correspondences between pools and measurable fractions

This section explains how we associate the simulated pools of each model with either the *POM* (particulate organic matter) fraction or the *MAOM* (mineral-associated organic matter) fraction. See Table S1 for a summary of the correspondences between the modeled pools and the *POM* and *MAOM* fractions.

We assume that the *POM* fraction (corresponding to the "light fraction" resulting from density fractionation) is composed of fragmented and partially processed plant litter which is not stabilized in the soil matrix through mineral association. We assume that the *MAOM* fraction (corresponding to the "heavy fraction" resulting from density fractionation) is composed of soil organic carbon which is enclosed in stable aggregates or strongly adsorbed to minerals. Since the live microbial biomass and dissolved organic carbon generally represent a small fraction of soil organic carbon, we can neglect them, so we assume they belong to neither *POM* nor *MAOM*.

S2.1. MEND

We assume that the *POM* fraction is composed of the $\mathrm{POM_O}$ and $\mathrm{POM_H}$ pools, and that the *MAOM* fraction is composed of the MOM and QOM pools.

List of organic carbon pools in the MEND-new (2022) model by G. Wang et al. (2022) (also see Figure S1):

- $\mathrm{POM_O}$ and $\mathrm{POM_H}$ (particulate organic matter decomposed by oxidative and hydrolytic enzymes, respectively).
- MOM (mineral-associated organic matter).
- QOM: "active layer of MOM" which can exchange carbon with DOM through adsorption and desorption (G. Wang et al., 2022).

- DOM (dissolved organic matter).
- MB_A and MB_D (active and dormant microbial biomass, respectively).
- EP_O, EP_H, EM: various microbial exo-enzymes.

Note that the "Litter" pool in the MEND model diagram in Figure S1 is not explicitly modeled as a pool, and therefore does not feature in the above list of organic carbon pools.

S2.2. Millennial

We assume that the measured *MAOM* fraction is the sum of the Aggregate C and MAOM pools, and that the *POM* fraction is entirely composed of the POM pool.

List of organic carbon pools in Millennial v2 by Abramoff et al. (2022) (see also Figure S2):

- POM (particulate organic carbon).
- Aggregate C: "stable microaggregates which remain after dispersion in the larger particle size fraction (>50–60 μm)" (Abramoff et al., 2022), so this corresponds to the coarse heavy fraction.
- MAOM (mineral-associated organic carbon): consists of organic matter associated to minerals through sorption (Abramoff et al., 2022).
- Microbial Biomass: live microbial biomass.
- LMWC (low molecular weight carbon): "LMWC could be analogous to dissolved organic C (DOC) if there is enough moisture in the soil matrix, and if we do not consider DOC molecules that are too large to be taken up by microbes" (Abramoff et al., 2022).

S2.3. SOMic

The *MAOM* fraction is composed of the MAC pool, and the *POM* fraction is composed of the SPM and IPM pools.

List of organic carbon pools in SOMic 1.0 by Woolf and Lehmann (2019) (also see Figure S3):

- SPM and IPM (soluble and insoluble plant matter, respectively).
- MAC (mineral-associated carbon): "mineral-sorbed or -occluded SOC" (Woolf & Lehmann, 2019).
- DOC (dissolved organic carbon).
- MB (microbial biomass).

S2.4. CORPSE

We associate the *MAOM* fraction with the $\mathrm{SPC_p}$, $\mathrm{CPC_p}$, and $\mathrm{MN_p}$ pools, since they represent mineral-adsorbed and micro-aggregated carbon (Moore et al., 2020). We associate the *POM* fraction with the $\mathrm{SPC_u}$ and $\mathrm{CPC_u}$ pools, but not the microbial $\mathrm{MN_u}$ pool, because POM is mostly composed of unprotected plant-derived carbon.

List of organic carbon pools in the CORPSE-fire-response version of the CORPSE model, first published in Sulman et al. (2014) and last updated in Moore et al. (2020) (see also Figure S4):

- $\mathrm{SPC_u}$, $\mathrm{CPC_u}$, and $\mathrm{MN_u}$ (Unprotected simple plant carbon, Unprotected complex plant carbon, and Unprotected microbe necromass, respectively).
- $\mathrm{SPC_p}$, $\mathrm{CPC_p}$, and $\mathrm{MN_p}$ (Protected simple plant carbon, Protected complex plant carbon, and Protected microbe necromass): "protected organic matter is inaccessible to microbial

decomposition through chemical sorption to mineral surfaces or occlusion within microaggregates" (Moore et al., 2020).

- LMB (live microbial biomass).

S2.5. MIMICS

According to Kyker-Snowman et al. (2020), the $\mathrm{SOM_c}$ pool corresponds to the *POM* fraction, and the $\mathrm{SOM_p}$ pool corresponds to the *MAOM* fraction.

List of organic carbon pools in MIMICS-CN v1.0 by Kyker-Snowman et al. (2020) (see also Figure S5):

- $\mathrm{LIT_m}$ and $\mathrm{LIT_s}$ (metabolic and structural litter, respectively): litter pools which are not considered part of soil organic matter.
- $\mathrm{SOM_p}$ (physicochemically protected soil organic matter): "is primarily composed of microbial products that are adsorbed onto mineral surfaces" and is "analogous to heavy fraction or MAOM pools" (Kyker-Snowman et al., 2020).
- $\mathrm{SOM_c}$ (chemically recalcitrant soil organic matter): "consists of decomposed or partially decomposed litter" and is "analogous to light fraction or POM pools" (Kyker-Snowman et al., 2020).
- $\mathrm{SOM_a}$ (available soil organic matter): "the only SOM pool that is available for microbial decomposition; it contains a mixture of fresh microbial residues, products that are desorbed from the SOMp pool (e.g., Jilling et al., 2018), as well as depolymerized organic matter from the SOMc pool" (Kyker-Snowman et al., 2020). This pool is usually very small and we associate it to neither POM nor MAOM.

- $\mathrm{MIC_r}$ and $\mathrm{MIC_K}$ ("low-efficiency, r strategist" microbes and "high-efficiency, K strategist" microbes, respectively): live microbial biomass pools.

Note that MIMICS-CN v1.0 also has a Dissolved Inorganic Nitrogen (DIN) pool, which does not contain organic carbon.

S3. Radiocarbon predictions with non-isotopic models

Among the new-generation models selected for this study, SOMic, MIMICS, and MEND have already implemented ^{14}C. However, the most recent and only open-source version of MEND does not include ^{14}C, and SOMic and MIMICS incorrectly implemented their ^{14}C simulations (see section S4). Nevertheless, we can still produce ^{14}C predictions with non-isotopic models by individually tracking the carbon fluxes at every time step and attaching a ^{14}C signal to each flux. Since none of the models define an internal structure for their pools, we will assume by default that the pools are well-mixed, which means that the Δ^{14}C of a pool's outflux is equal to the pool's Δ^{14}C. This assumption is common practice for ^{14}C modeling in soils (Sierra et al., 2017).

We run all of the selected models using the forward Euler method to advance from one time step to the next. The models either implicitly or explicitly produce the internal flux matrix Φ^i at each time step i, where $\Phi^i_{jk} \geq 0$ is the flux of carbon from pool k into pool j (with $j \neq k$), and $\Phi^i_{jj} \leq 0$ is the total outflux of carbon out of pool j at time step i. They also define the external influx vector I^i such that $I^i_j \geq 0$ is the influx of carbon entering the modeled system through pool j at time step i. Matrix Φ contains all the fluxes between the pools and out of the system, and vector I contains all the influxes of carbon from outside the system into the modeled pools. We can therefore find the carbon stocks C^{i+1}_j of pool j at time step $i+1$ based on the Φ^i, I^i, and C^i_j of the previous time step i:

$$C^{i+1}_j = C^i_j + I^i_j + \sum_k \Phi^i_{jk}\,, \tag{S1}$$

where the summation of internal fluxes Φ^i_{jk} is performed over all donor pools k to get the total internal carbon flux into pool j (when $k \neq j$), subtracted by the flux out of pool j (when $k = j$).

Assuming the pools are well-mixed, we can now produce ^{14}C predictions by tagging each flux Φ_{jk} with the ^{14}C signal of pool k. We measure the ^{14}C signal in terms of the unitless "absolute Fraction Modern" ($\mathrm{FM_{abs}}$) as defined in Trumbore, Sierra, and Hicks Pries (2016), such that $\mathrm{FM_{abs}} = 1 + (\Delta^{14}\mathrm{C}/1000‰)$. The $\mathrm{FM_{abs}}$ is proportional to the ^{14}C/^{12}C ratio normalized to a δ^{13}C of $-25‰$ (Trumbore et al., 2016), and is thus proportional to the normalized ratio of ^{14}C to total carbon (^{14}C/C), considering the negligible abundance of ^{14}C compared to ^{12}C and ^{13}C. Therefore, if we know F^i_j, the $\mathrm{FM_{abs}}$ of pool j at time step i, we can find F^{i+1}_j at time step $i+1$ with the following equation (provided all the pools and the influx have comparable δ^{13}C signals):

$$F^{i+1}_j C^{i+1}_j = (1-\lambda) F^i_j C^i_j + I^i_j F^i_{\mathrm{influx}} + \sum_k \Phi^i_{jk} F^i_k \,, \tag{S2}$$

where C^{i+1}_j is given by equation (S1), λ is the radioactive decay rate of ^{14}C in units of inverse time step size, and F^i_{influx} is the $\mathrm{FM_{abs}}$ of the external carbon influx at time step i given by the forcing data. We can then recover the Δ^{14}C at each time step i and for each pool j with $(F^i_j - 1) \times 1000‰$.

S4. Incorrect or inaccurate ^{14}C implementations

S4.1. SOMic

The SOMic model (Woolf & Lehmann, 2019), as implemented on the GitHub repository `domwoolf/somic1` (commit `be34e56` from June 2019), does not produce accurate ^{14}C predictions. Instead of working with the more typical Δ^{14}C or absolute Fraction Modern ($\mathrm{FM_{abs}}$) units, this implementation tracks the ^{14}C age, which we summarily define as $\mathrm{Age} = -\log(\mathrm{FM_{abs}})\,\lambda^{-1}$, where λ is the radioactive decay rate of ^{14}C. This causes complications when updating the ^{14}C ages of the pools at each time step and when computing the total ^{14}C age of the soil from the ^{14}C ages of the individual pools. Indeed, to find the combined age $\mathrm{Age_{A+B}}$ of pools A and B, the implementation of SOMic takes a weighted average over the ages, which is not entirely accurate:

$$\mathrm{Age_{A+B}} = \frac{C_\mathrm{A}\mathrm{Age_A} + C_\mathrm{B}\mathrm{Age_B}}{C_\mathrm{A} + C_\mathrm{B}}\,, \tag{S3}$$

where Age_i and C_i are the ^{14}C age and the carbon stocks, respectively, of pool i. This weighted average formula is used to integrate the ^{14}C ages of carbon fluxes into the pools at each time step on lines 154-160, and to compute the ^{14}C age of the total soil on line 210 of file `src/SOMIC.cpp` in the `domwoolf/somic1` GitHub repository (commit `be34e56`).

In order to prove that equation (S3) is inaccurate, let us derive how to correctly add the ^{14}C ages of pools A and B. Let $^{14}C_i$ denote the ^{14}C stocks and C_i the total carbon stocks of pool i. Then, by conservation of mass, we have

$$^{14}C_\mathrm{A+B} = {}^{14}C_\mathrm{A} + {}^{14}C_\mathrm{B} \quad \text{and} \quad C_\mathrm{A+B} = C_\mathrm{A} + C_\mathrm{B} \quad \Rightarrow \quad \frac{^{14}C_\mathrm{A+B}}{C_\mathrm{A+B}} = \frac{^{14}C_\mathrm{A} + {}^{14}C_\mathrm{B}}{C_\mathrm{A} + C_\mathrm{B}}\,. \tag{S4}$$

Since the FM_{abs} is proportional to the $^{14}C/C$ ratio (assuming pools A and B have a similar ^{13}C content), the above is equivalent to

$$F_{A+B} = \frac{C_A F_A + C_B F_B}{C_A + C_B}\,, \tag{S5}$$

where F_i and C_i are the FM_{abs} and carbon stocks, respectively, of pool i. It follows that the combined ^{14}C age of pools A and B is given by

$$\mathrm{Age}_{A+B} = -\lambda^{-1} \cdot \log\left(\frac{C_A \exp(-\lambda \cdot \mathrm{Age}_A) + C_B \exp(-\lambda \cdot \mathrm{Age}_B)}{C_A + C_B}\right). \tag{S6}$$

Notice that equation (S3) is the first non-zero term of the above result's Taylor expansion around $\mathrm{Age}_A = 0$, $\mathrm{Age}_B = 0$. This means that equation (S3) works well for ages that are close to zero, i.e. when the $\Delta^{14}C$ is close to zero. However, it fails to accurately predict the propagation of the bomb spike into the soil ecosystem in the latter half of the 20th century, as shown in Figure S6. While the error induced by the incorrect implementation exceeds 25‰ for the total soil $\Delta^{14}C$ in the 1970s, the error in the 2000s and 2010s is only around 10‰, which is relatively minor.

S4.2. MIMICS

The only MIMICS version already implemented with ^{14}C is published in Y. Wang et al. (2021), and the code is available at `https://data.csiro.au/collection/csiro:47942v1`. However, this ^{14}C implementation is incorrect (see Figure S7).

The time evolution of the carbon stocks in MIMICS is given by function $f(C,t)$, which depends on the carbon stocks vector C and time t. Function f is implemented as subroutine `modelx` in the source file `vsoilmic05f_ms25.f90`. We can write function f in terms of internal carbon transfer matrix A and carbon influx vector I:

$$\mathrm{d}C/\mathrm{d}t = f(C,t) = A(C,t)C + I(t)\,, \tag{S7}$$

where matrix $A(C,t)$ is a function of carbon stocks C and time t, and vector $I(t)$ is time-dependent.

Then, following the same procedure which yielded equation (S2), we can derive the equation governing the evolution of the ^{14}C stocks (^{14}C):

$$\mathrm{d}^{14}C/\mathrm{d}t = -\lambda^{14}C + A(C,t)^{14}C + {}^{14}I(t)\,, \tag{S8}$$

where λ is the radioactive decay rate of ^{14}C, and ^{14}I is the external influx of ^{14}C.

However, in the ^{14}C-implementation of MIMICS, the evolution of the ^{14}C stocks is predicted with

$$\mathrm{d}^{14}C/\mathrm{d}t = -\lambda^{14}C + f(^{14}C,t) = -\lambda^{14}C + A(^{14}C,t)^{14}C + {}^{14}I(t)\,. \tag{S9}$$

The above equation is incorrect because $A(^{14}C,t) \neq A(C,t)$.

S5. Turnover times in the Millennial model

In Millennial version 2 (Abramoff et al., 2022), the POM, MAOM, and Aggregate C pools exchange carbon with each other on the scale of a few months. The aggregate formation rate of the POM pool is between 0.012/day and 0.026/day (k_{pa} in Table A1 of Abramoff et al., 2022), which translates to an average aggregation time of 1-3 months. Meanwhile, the optimized rate of aggregate formation for the MAOM pool is between 0.0038/day and 0.0052/day (k_{ma} in Table A1 of Abramoff et al., 2022), giving MAOM an average aggregation time of 6-8 months. The Aggregate C pool has a breakdown rate of around 0.02/day (k_b in Table A1 of Abramoff et al., 2022), so aggregates have a turnover time of just 50 days. POM and MAOM exchange their carbon rapidly with the Aggregate C pool, which then redistributes the carbon back to the POM and MAOM pools in less than 2 months, on average. This means that the ^{14}C signals of the POM, MAOM, and Aggregate C pools get homogenized within a couple years.

References

Abramoff, R. Z., Guenet, B., Zhang, H., Georgiou, K., Xu, X., Viscarra Rossel, R. A., ... Ciais, P. (2022, January). Improved global-scale predictions of soil carbon stocks with Millennial Version 2. *Soil Biology and Biochemistry*, *164*, 108466. Retrieved 2022-01-19, from https://linkinghub.elsevier.com/retrieve/pii/S0038071721003400 doi: 10.1016/j.soilbio.2021.108466

Graven, H., Allison, C. E., Etheridge, D. M., Hammer, S., Keeling, R. F., Levin, I., ... White, J. W. C. (2017, December). Compiled records of carbon isotopes in atmospheric CO_2 for historical simulations in CMIP6. *Geoscientific Model Development*, *10*(12), 4405–4417. Retrieved 2021-03-10, from https://gmd.copernicus.org/articles/10/4405/2017/ doi: 10.5194/gmd-10-4405-2017

Kyker-Snowman, E., Wieder, W. R., Frey, S. D., & Grandy, A. S. (2020, September). Stoichiometrically coupled carbon and nitrogen cycling in the MIcrobial-MIneral Carbon Stabilization model version 1.0 (MIMICS-CN v1.0). *Geoscientific Model Development*, *13*(9), 4413–4434. Retrieved 2023-06-29, from https://gmd.copernicus.org/articles/13/4413/2020/ doi: 10.5194/gmd-13-4413-2020

Moore, J. A. M., Sulman, B. N., Mayes, M. A., Patterson, C. M., & Classen, A. T. (2020, April). Plant roots stimulate the decomposition of complex, but not simple, soil carbon. *Functional Ecology*, *34*(4), 899–910. Retrieved 2022-08-29, from https://onlinelibrary.wiley.com/doi/10.1111/1365-2435.13510 doi: 10.1111/1365-2435.13510

Sierra, C. A., Müller, M., Metzler, H., Manzoni, S., & Trumbore, S. E. (2017, May). The muddle of ages, turnover, transit, and residence times in the carbon cycle. *Global*

Change Biology, *23*(5), 1763–1773. Retrieved 2021-04-09, from http://doi.wiley.com/10.1111/gcb.13556 doi: 10.1111/gcb.13556

Sulman, B. N., Phillips, R. P., Oishi, A. C., Shevliakova, E., & Pacala, S. W. (2014, December). Microbe-driven turnover offsets mineral-mediated storage of soil carbon under elevated CO2. *Nature Climate Change*, *4*(12), 1099–1102. Retrieved 2022-05-29, from http://www.nature.com/articles/nclimate2436 doi: 10.1038/nclimate2436

Trumbore, S. E., Sierra, C. A., & Hicks Pries, C. E. (2016). Radiocarbon Nomenclature, Theory, Models, and Interpretation: Measuring Age, Determining Cycling Rates, and Tracing Source Pools. In E. A. Schuur, E. Druffel, & S. E. Trumbore (Eds.), *Radiocarbon and Climate Change* (pp. 45–82). Cham: Springer International Publishing. Retrieved 2021-04-05, from http://link.springer.com/10.1007/978-3-319-25643-6_3 doi: 10.1007/978-3-319-25643-6_3

Wang, G., Gao, Q., Yang, Y., Hobbie, S. E., Reich, P. B., & Zhou, J. (2022, March). Soil enzymes as indicators of soil function: A step toward greater realism in microbial ecological modeling. *Global Change Biology*, *28*(5), 1935–1950. Retrieved 2023-06-23, from https://onlinelibrary.wiley.com/doi/10.1111/gcb.16036 doi: 10.1111/gcb.16036

Wang, Y., Zhang, H., Ciais, P., Goll, D., Huang, Y., Wood, J. D., ... Prescher, A. (2021, April). Microbial Activity and Root Carbon Inputs Are More Important than Soil Carbon Diffusion in Simulating Soil Carbon Profiles. *Journal of Geophysical Research: Biogeosciences*, *126*(4). Retrieved 2022-07-10, from https://onlinelibrary.wiley.com/doi/10.1029/2020JG006205 doi: 10.1029/

2020JG006205

Woolf, D., & Lehmann, J. (2019, December). Microbial models with minimal mineral protection can explain long-term soil organic carbon persistence. *Scientific Reports*, *9*(1), 6522. Retrieved 2021-10-01, from http://www.nature.com/articles/s41598-019-43026-8 doi: 10.1038/s41598-019-43026-8

Table S1. Correspondences between simulated carbon pools and the POM fraction, MAOM fraction, or other carbon reservoirs.

Model	POM fraction	MAOM fraction	Other SOC pools	Litter pools
MEND	POM_O, POM_H	MOM, QOM	DOM, MB_A, MB_D, EP_O, EP_H, EM	
Millennial	POM	MAOM, Aggregate C	LMWC, Microbial Biomass	
SOMic	SPM, IPM	MAC	DOC, MB	
CORPSE	SPC_u, CPC_u	SPC_p, CPC_p, MN_p	MN_u, LMB	
MIMICS	SOM_c	SOM_p	SOM_a, MIC_r, MIC_K	LIT_m, LIT_s

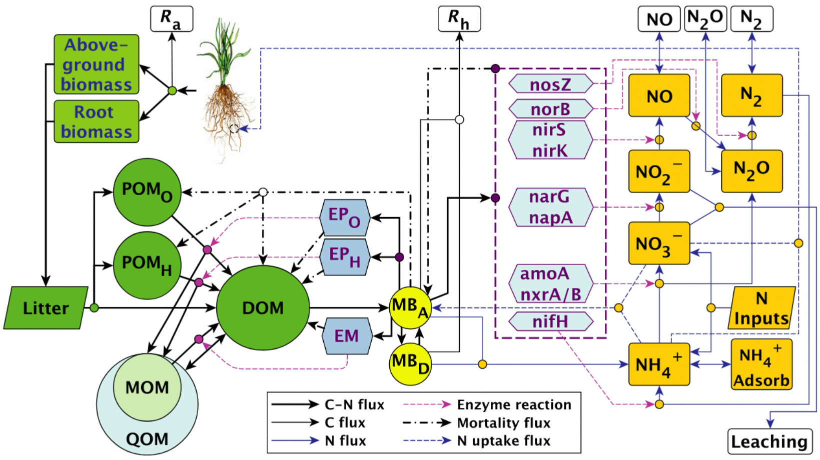

Figure S1. MEND-new (2022) model diagram from G. Wang et al. (2022)

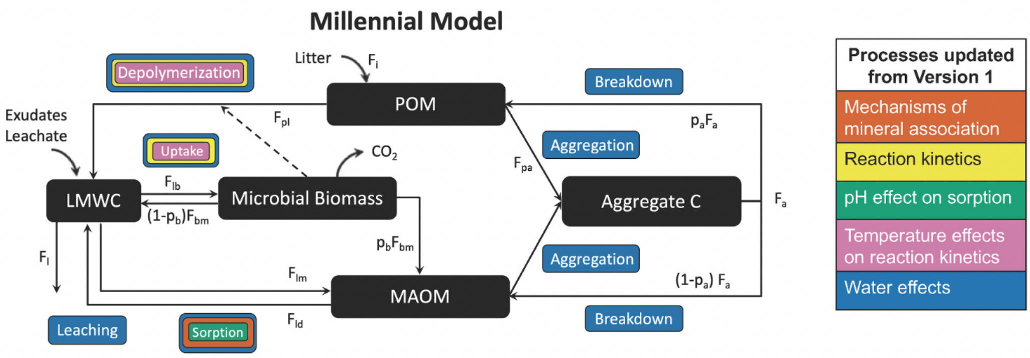

Figure S2. Millennial V2 diagram from Abramoff et al. (2022)

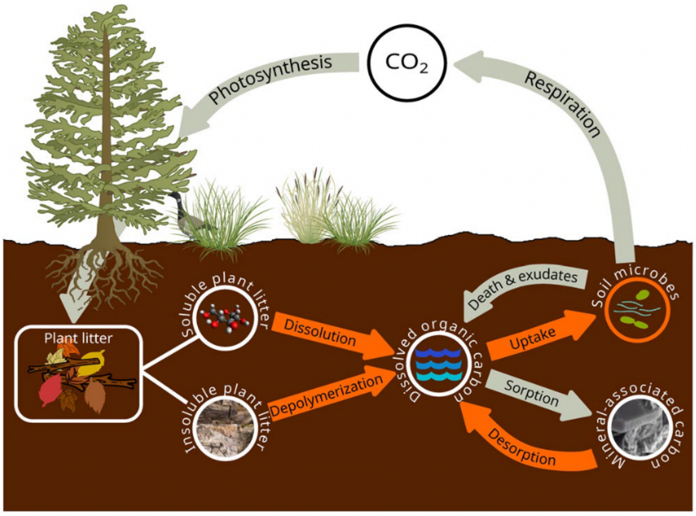

Figure S3. SOMic 1.0 diagram from Woolf and Lehmann (2019)

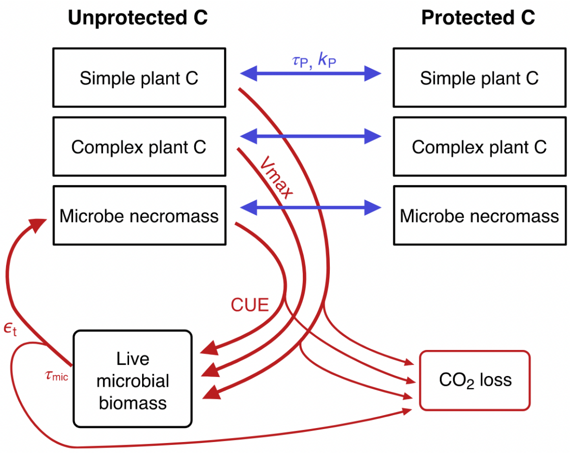

Figure S4. CORPSE diagram from Moore et al. (2020)

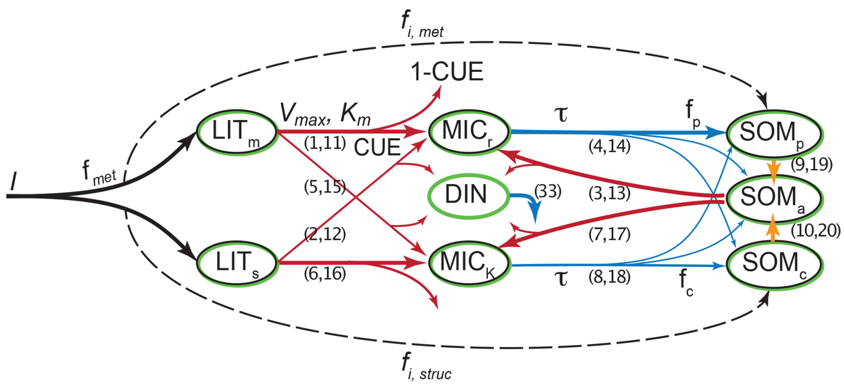

Figure S5. MIMICS-CN v1.0 diagram from Kyker-Snowman et al. (2020)

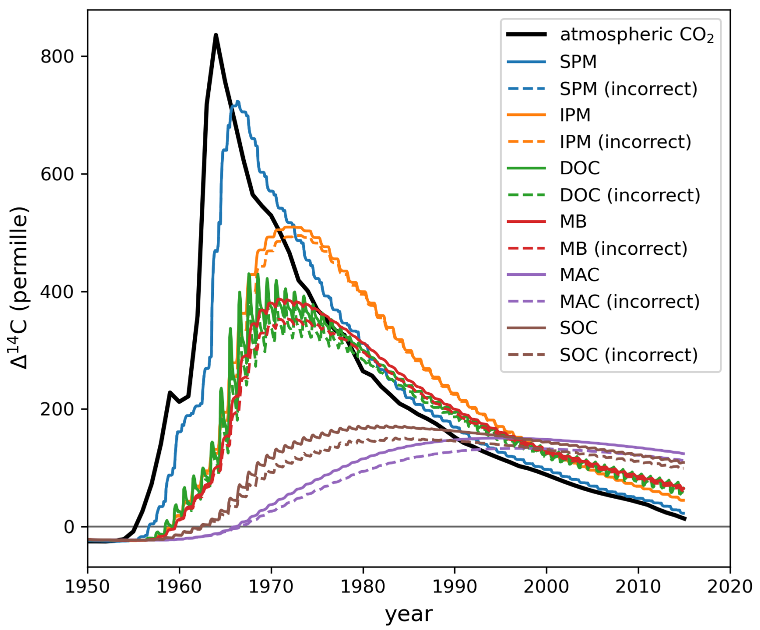

Figure S6. Comparison of $\Delta^{14}C$ predicted by SOMic with the correct and incorrect ^{14}C implementations. The atmospheric $\Delta^{14}CO_2$ of the Northern Hemisphere (source: Graven et al., 2017) is plotted for reference. SOMic pool names: SPM, soluble plant matter; IPM, insoluble plant matter; DOC, dissolved organic carbon; MB, microbial biomass; MAC, mineral-associated carbon; SOC, total soil organic carbon.

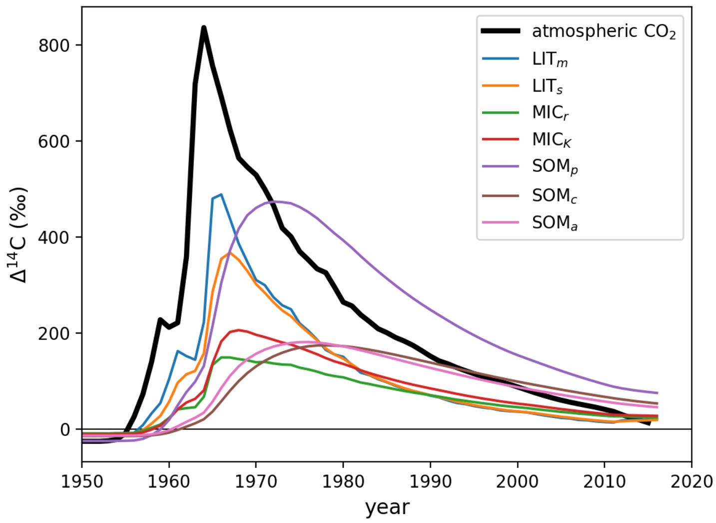

Figure S7. $\Delta^{14}C$ output of MIMICS (Y. Wang et al., 2021) with incorrect isotopic implementation. The atmospheric $\Delta^{14}CO_2$ of the Northern Hemisphere (source: Graven et al., 2017) is plotted for reference. MIMICS pool names: LIT_m, metabolic litter; LIT_s, structural litter; MIC_r, r-strategist microbes; MIC_K, K-strategist microbes; SOM_p, physically protected soil organic matter; SOM_c, chemically protected soil organic matter; SOM_a, active soil organic matter.

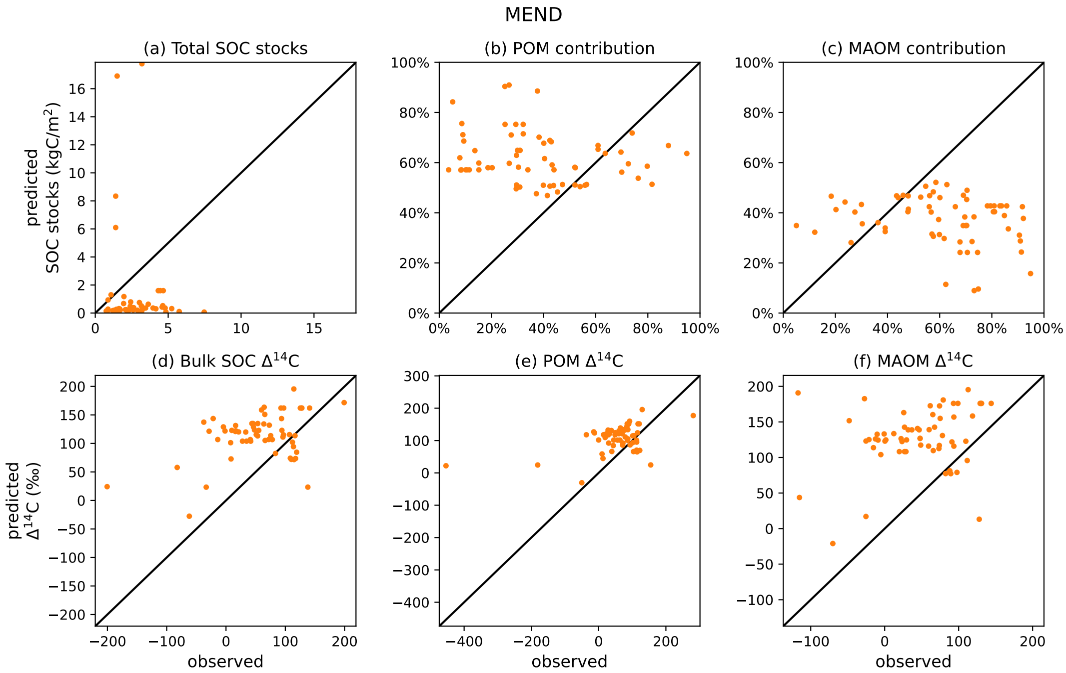

Figure S8. Predictions vs observations plots for the MEND model.

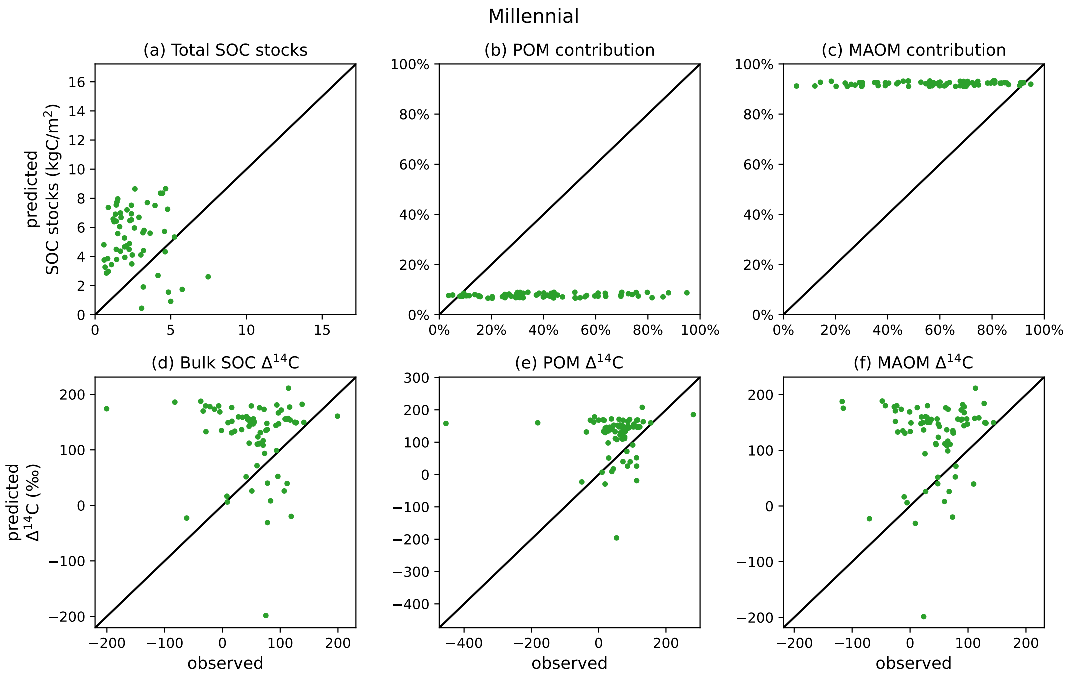

Figure S9. Predictions vs observations plots for the Millennail model.

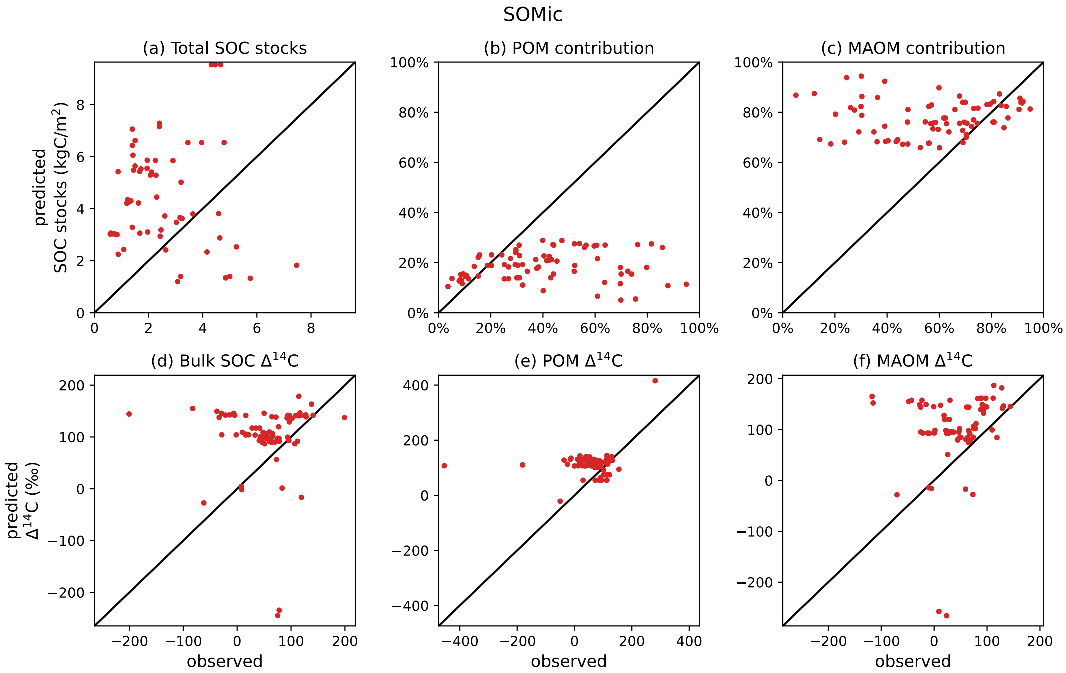

Figure S10. Predictions vs observations plots for the SOMic model.

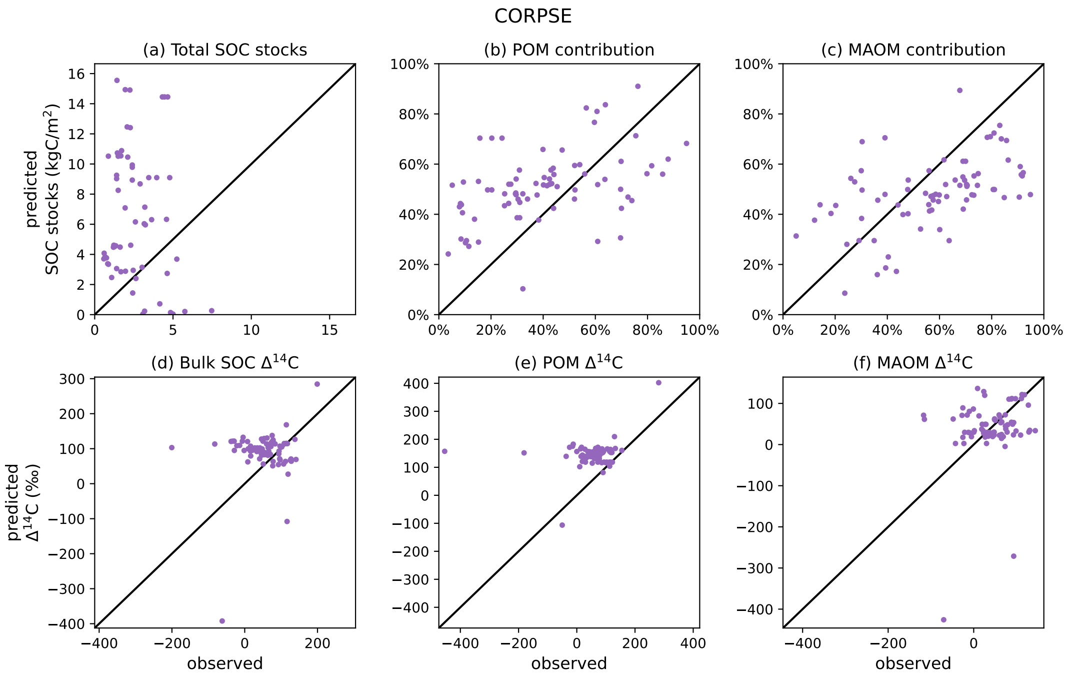

Figure S11. Predictions vs observations plots for the CORPSE model.

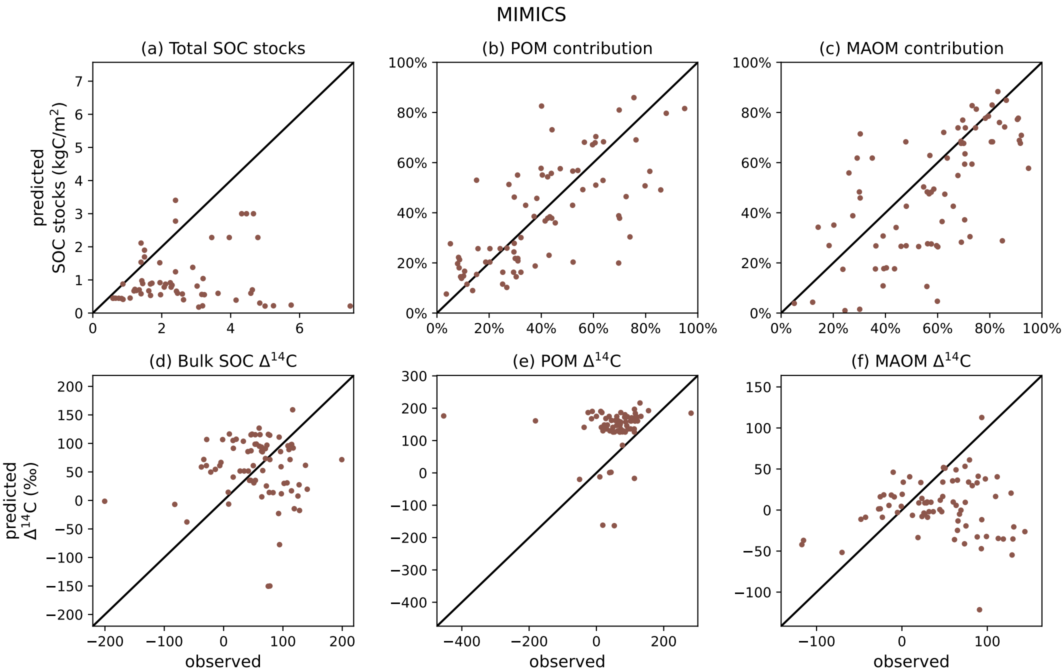

Figure S12. Predictions vs observations plots for the MIMICS model.